

A Kustaanheimo–Stiefel regularization of the elliptic restricted three-body problem and the detection of close encounters with fast Lyapunov indicators

Mattia Rossi ^{a,b}, Massimiliano Guzzo ^{a,*}

^a Università degli Studi di Padova, Dipartimento di Matematica “Tullio Levi-Civita”, Via Trieste, 63 35121 Padova, Italy

^b Università degli Studi di Genova, MIDA – Dipartimento di Matematica, Via Dodecaneso, 35 16146 Genova, Italy

ARTICLE INFO

Communicated by A. Celletti

Dataset link: nssdc.gsfc.nasa.gov/planetary/factsheet/

Keywords:

Celestial mechanics
Astrodynamics
Elliptic restricted 3-body problem
Kustaanheimo–Stiefel regularization
Fast Lyapunov indicators
Hill's sphere

ABSTRACT

We present the Kustaanheimo–Stiefel (KS) regularization of the elliptic restricted three-body problem (ER3BP) at the secondary body P_2 , and discuss its use to study a category of transits through its Hill's sphere (fast close encounters). Starting from the Hamiltonian representation of the problem using the synodic rotating–pulsating reference frame and the true anomaly of P_2 as independent variable, we perform the regularization at the secondary body analogous to the circular case by applying the classical KS transformation and the iso-energetic reduction in an extended 10-dimensional phase-space; this translates into an efficient algorithm that can be readily implemented to numerically integrate the equations of motion. Using such a regularized Hamiltonian we recover a definition of fast close encounters in the ER3BP for small values of the mass parameter μ (while we do not require a smallness condition on the eccentricity of the primaries), and we show that for these encounters the solutions of the variational equations are characterized by an exponential growth during the fast transits through the Hill's sphere. Thus, for small μ , we justify the effectiveness of the regularized fast Lyapunov indicators (RFLIs) to detect orbits with multiple fast close encounters. Finally, we provide numerical demonstrations and show the benefits of the regularization in terms of the computational cost.

1. Introduction

The regularization of the gravitational singularities, appeared at the beginning of the XXth century, has become in the last decades an extremely useful technique to deal with the numerical integration of the N-body problems. Particularly two kinds of regularization techniques are widely known: a geometric one, which basically aims at modifying the equations of motion such that they are defined and regular even on the singularities, and a solution-based one, whose goal consists in an analytic continuation of the original solution through the singular point. In this paper we focus precisely on a celebrated example of the former category, i.e., the Kustaanheimo–Stiefel regularization for a special case of utmost importance, represented by the restricted three-body problem, originally in its circular (CR3BP) and then elliptic (ER3BP) variant.

In a seminal paper [2] Levi-Civita performed a local¹ regularization of the planar CR3BP, which relies on the conservation of the so-called Jacobi integral, through the introduction of canonical transformations and a time reparametrization that nowadays are known, after his name, as Levi-Civita (LC) regularization. The issue for the spatial CR3BP was solved by Kustaanheimo and Stiefel in the mid-1960s [3,4]. The

latter procedure is more complicated than the LC one since it exploits a projection map from a space of four redundant variables to the three-dimensional Cartesian space. Both LC and KS regularizations are *iso-energetic*, since they exploit the existence of a global first integral, the so-called Jacobi constant. There exist in the literature many uses of the KS transformation to regularize binary collisions in the general 3-body and N-body problems, as well as perturbations of the Kepler problem whose definitions include restricted problems more general than the CR3BP and ER3BP (see [5] and, for example, [6–13] and references therein). For the ER3BP (and for more general restricted problems) a 10-dimensional phase-space is required. In fact, in addition to the 8-dimensional phase-space of the KS variables and an additional variable corresponding to the physical time, another variable corresponding to the energy of the system (variable in time for the ER3BP) is required. While these approaches include the regularizations of the ER3BP, the geometric properties of this system provide specific representations which are more adapted, for example, to the computation of ejection-collision orbits or the dynamics at the Lagrangian points (see, e.g., [14,15]) and, as we consider in this paper, the study of fast close encounters with the secondary body P_2 .

* Corresponding author.

E-mail addresses: mrossi@math.unipd.it, rossi.ma@dima.unige.it (M. Rossi), guzzo@math.unipd.it (M. Guzzo).

¹ In case of multiple singularities the term refers to the deletion of only one of them at a time, as opposed to a global method, mainly due to Birkhoff [1].

We remark that specific approaches to the regularization of the ER3BP have been developed also using regularizations different from the KS one. Formulations in this regard have been derived in [14,16] and applied in [17,18] for the planar setting; in [19–22] for the spatial one.

A convenient formulation of the ER3BP uses a synodic rotating–pulsating reference frame and the true anomaly of the secondary body as independent variable [14]. Consider an ER3BP defined by the motion of a body P of negligible mass in the gravitation field of two massive bodies P_1 (the primary) and P_2 (the secondary) performing an elliptic Keplerian motion of eccentricity $\varepsilon \in (0, 1)$. As usual, the simplifying assumptions on the units correspond to setting $m_1 = 1 - \mu$, $m_2 = \mu$ for $\mu \in (0, 1/2)$ as the masses of P_1 , P_2 respectively, while $a = 1$ and $T = 2\pi$ are the semi-major axis and the period of the elliptic motion. By denoting with (x, y, z) , (p_1, p_2, p_3) the coordinates of P and their conjugate momenta, and with f the true anomaly of the elliptic motion of P_2 which is used as independent variable, the Hamiltonian reads:

$$\mathcal{H}(x, y, z, p_1, p_2, p_3, f) = \frac{1}{2}(p_1^2 + p_2^2 + p_3^2) + p_1 y - x p_2 - \frac{1}{1 + \varepsilon \cos f} \left(\frac{1 - \mu}{d_1} + \frac{\mu}{d_2} - \frac{1}{2}(x^2 + y^2 + z^2) \varepsilon \cos f \right), \quad (1)$$

where $d_1 = \|P - P_1\|$, $d_2 = \|P - P_2\|$. In this paper we first represent the KS regularization at the secondary body of the Hamiltonian (1) by applying the classical KS transformation and the iso-energetic reduction in the extended 10-dimensional phase-space. First, we provide indeed a simple and self-consistent proof on the projection of the solutions of the regularized Hamiltonian to the original solutions, by adapting to the elliptic case a derivation of the KS Hamiltonian of the CR3BP given in [23]. This leads to a KS algorithm, which is explained and provided in full detail in Section 4.1, to numerically compute the flow of the ER3BP. We also assess the effectiveness of the regularization for numerical integrations, and the advantage in terms of numerical performances, in a fictitious simple scenario which is nevertheless representative (for the choice of the initial conditions) of realistic close encounters in the Solar System, such as the non-coplanar close encounters with Jupiter, in the Sun-Jupiter ER3BP. Finally, we use the regularized Hamiltonian to extend the definition of fast close encounters to the ER3BP, and justify the effectiveness of the RFLIs to detect orbits with multiple of such fast close encounters.

We call ‘close encounter’ a transit of a solution $(x(f), y(f), z(f))$ of the ER3BP through the Hill’s sphere of P_2 occurring in any finite interval $[f_1, f_2]$ of the true anomaly f (collision solutions are not included). We consider values of the mass parameter $\mu \leq 1/10$ and we define the Hill’s sphere of P_2 by:

$$B(\mu^{\frac{1}{3}}) = \{(x, y, z) \in \mathbb{R}^3 : d_2 < \mu^{\frac{1}{3}}\}.$$

Notice that this definition of Hill’s sphere is different from the conventional one by a numerical factor: the radius $\mu^{\frac{1}{3}}$ corresponds to $3^{\frac{1}{3}} r_h$, where r_h is the usual Hill’s radius. A close encounter occurring for $f \in [f_1, f_2]$ satisfies $d_2(f_1) = d_2(f_2) = \mu^{\frac{1}{3}}$ as well as $0 < d_2(f) < \mu^{\frac{1}{3}}$ for all $f \in (f_1, f_2)$.

We consider the category, critical for the numerical integrations, of fast close encounters, generalizing the conditions of fast close encounters which are given for the CR3BP. We recall that fast close encounters are frequently observed for celestial bodies in the Solar System (see for example [24,25], where the dynamics of comet 67P Churyumov-Gerasimenko, target of the recent Rosetta mission, is discussed in detail), and they are important also for the study of the risk of impact of asteroids on the Earth, as well as for the technique of gravity assist to change the energy of a spacecraft.

Fast close encounters are easily identified in the CR3BP by the encounters occurring for values of the Jacobi constant C satisfying:

$$\gamma := \frac{3 - 4\mu + \mu^2 - C}{2} > 0, \quad (2)$$

with the exclusion of a neighborhood of $\gamma = 0$. The condition (2) (or similar ones), which appeared in several studies of close encounters with Levi-Civita regularization (see, e.g., [26–30]) as well as in the heuristic approach known as Öpik’s theory (see [31], revised in [32]), is understood by representing the Hamiltonian of the planar CR3BP, Levi-Civita regularized at P_2 , in the form:

$$\mathcal{K}(u, U) = \frac{1}{8} \|U - b(u)\|^2 - \|u\|^2 \left(\frac{3 - 4\mu + \mu^2 - C}{2} \right) - \mu + \mathcal{R}_6(u), \quad (3)$$

where (u_1, u_2) are the Levi-Civita coordinates and $U = (U_1, U_2)$ are the momenta conjugate to $u = (u_1, u_2)$ defined as in [2]; $b(u) = (b_1(u), b_2(u))$ is cubic in the u ; $\mathcal{R}_6(u)$ is regular at $u = 0$ with Taylor expansion which begins with order 6. If $\gamma > 0$, the coefficient of $\|u\|^2$ in the Levi-Civita Hamiltonian (3) is strictly negative, allowing to use methods of hyperbolic dynamics to study the fast close encounters of the CR3BP, as it was done in [26,27,29] with analytic methods, and in [28] to study the effectiveness of RFLIs to detect orbits with multiple close encounters in the planar CR3BP. We remark that, by considering the higher order corrections to the quadratic approximation of the Hamiltonian, a neighborhood of the limit case $\gamma = 0$ should be avoided.

To understand heuristically why the condition $\gamma > 0$ (with the exclusion of a neighborhood of $\gamma = 0$) represents the condition of fast close encounters, consider a body P having a close encounter with P_2 : P arrives at a small distance ρ from P_2 with velocity v (in the rotating frame) satisfying:

$$\|v\|^2 = x^2 + y^2 + 2 \frac{1 - \mu}{d_1} + 2 \frac{\mu}{d_2} - C \sim 3 - C + 2 \frac{\mu}{d_2} + \mathcal{O}(\rho).$$

For the small distances ρ such that μ/d_2 is still negligible with respect to 1, for values of C such that $3 - C$ is of order 1 with respect to μ , we have that $\|v\| \approx \sqrt{3 - C} \approx \sqrt{2\gamma}$ is of order 1 as well, and consequently the encounter is fast. Alternative definitions of fast close encounters, as in Öpik’s theory, refer to the hyperbolic approximations of the Cartesian solutions which are obtained by considering the Keplerian motion defined by the secondary body P_2 .

Regularized fast Lyapunov indicators have been introduced in [28, 33,34] (see also [35], and references therein) and have been used in [28,36,37] to detect the several kinds of close encounters with the secondary body P_2 . The ability of FLIs to detect fast close encounters of the planar CR3BP [38,39], i.e., for $\gamma > 0$, has been related to the exponential growth of tangent vectors for orbits transiting suitably fast in the Hill’s sphere of the planet [28]. In fact, the Jacobian matrix $\mathcal{X}(u, U)$ of the Hamiltonian vector field of (3) computed in the limit:

$$\mathcal{X}_0 = \lim_{\|u\| \rightarrow 0, \|du/ds\| \rightarrow \sqrt{\mu/2}} \mathcal{X}(u, U),$$

where $s = s(t)$ is the Levi-Civita time reparametrization, has eigenvalues $\pm \sqrt{\gamma/2}$, and therefore the encounter is hyperbolic when $\gamma > 0$.

To develop this idea for the full ER3BP we consider the Hamiltonian $\mathcal{K}(u, \phi, U, \Phi)$ of the problem regularized at P_2 , as it will be obtained in Section 2: $u = (u_1, u_2, u_3, u_4)$ denote the KS variables; $U = (U_1, U_2, U_3, U_4)$ a set of conjugate momenta. The additional conjugate variables ϕ, Φ are needed in the regularization of the elliptic problem: by denoting with s the independent variable (the proper time) of the Hamilton equations of the regularized Hamiltonian, $\phi(s)$ is the true anomaly of P_2 for the value s of the proper time (see Section 2 for all the details). We obtain for $\mathcal{K}(u, \phi, U, \Phi)$ a representation similar to (3):

$$\mathcal{K}(u, \phi, U, \Phi) = \frac{1}{8} \|U - b(u)\|^2 - \|u\|^2 \left(-\Phi + \frac{3 - 4\mu + \mu^2}{2(1 + \varepsilon \cos \phi)} \right) - \frac{\mu}{1 + \varepsilon \cos \phi} + \mathcal{R}_6(u, \phi), \quad (4)$$

where $b(u) = \mathcal{O}(\|u\|^3) \in \mathbb{R}^4$; $\mathcal{R}_6(u, \phi)$ is regular at $u = 0$, and its Taylor expansion in the vector variable u begins with order 6. There is however a fundamental difference with respect to the circular case, since the coefficient:

$$\Gamma(\phi, \Phi) = -\Phi + \frac{3 - 4\mu + \mu^2}{2(1 + \varepsilon \cos \phi)} \quad (5)$$

depends on the variables Φ, ϕ , and therefore is not constant along the solutions $(u(s), \phi(s), U(s), \Phi(s))$ of the Hamilton equations of \mathcal{K} . Moreover, the derivative of $\Gamma_s := \Gamma(\phi(s), \Phi(s))$ with respect to the proper time s is proportional to ε , but does not vanish for $\mu \rightarrow 0$. Using the representation (4), we notice that the variation of Γ_s satisfies:

$$\frac{d}{ds} \Gamma_s = -\varepsilon \mu \frac{\sin \phi}{(1 + \varepsilon \cos \phi)^2} - \frac{\varepsilon \sin \phi}{(1 + \varepsilon \cos \phi)^2} \mathcal{O}(\|u\|^6),$$

so that, during the transit through the Hill's sphere, where $\|u\|$ is smaller than order $\mu^{\frac{1}{6}}$ (see (48) in Section 3), we have:

$$\left| \frac{d\Gamma_s}{ds} \right| = \mathcal{O}(\varepsilon \mu).$$

The stability of Γ_s up to times of the order of $1/(\varepsilon \mu)$ provides the opportunity to assess the hyperbolicity of fast close encounters for the ER3BP, for small values of μ . In fact, to establish the hyperbolic character of the close encounter in the ER3BP from the representation (4) we need to establish the stability of the coefficient Γ_s for two reasons. First, we notice that the variational matrix \mathcal{X} of the Hamiltonian vector field of \mathcal{K} has the representation:

$$\mathcal{X}(u, U, \phi) = \begin{pmatrix} \frac{\partial^2 \mathcal{K}}{\partial u \partial U} & \frac{\partial^2 \mathcal{K}}{\partial U \partial U} \\ -\frac{\partial^2 \mathcal{K}}{\partial u \partial u} & -\frac{\partial^2 \mathcal{K}}{\partial U \partial u} \end{pmatrix} = \mathcal{X}_0 + \mathcal{O}(\|u\|^2) + \mathcal{O}(\|U\|)\mathcal{O}(\|u\|), \quad (6)$$

with

$$\mathcal{X}_0 = \begin{pmatrix} 0 & 0 & 0 & 0 & 1/4 & 0 & 0 & 0 \\ 0 & 0 & 0 & 0 & 0 & 1/4 & 0 & 0 \\ 0 & 0 & 0 & 0 & 0 & 0 & 1/4 & 0 \\ 0 & 0 & 0 & 0 & 0 & 0 & 0 & 1/4 \\ 2\Gamma_s & 0 & 0 & 0 & 0 & 0 & 0 & 0 \\ 0 & 2\Gamma_s & 0 & 0 & 0 & 0 & 0 & 0 \\ 0 & 0 & 2\Gamma_s & 0 & 0 & 0 & 0 & 0 \\ 0 & 0 & 0 & 2\Gamma_s & 0 & 0 & 0 & 0 \end{pmatrix}. \quad (7)$$

Therefore, on one hand we need that motions entering the Hill's sphere with $\Gamma_0 > 0$, maintain a value of $\Gamma_s > 0$ during the transit through the Hill's sphere, so that the matrix \mathcal{X}_0 is hyperbolic.² On the other hand, we need to provide an upper bound to the elements of the matrix $\mathcal{X} - \mathcal{X}_0$ during the transit in the Hill's sphere, to ensure the hyperbolicity of \mathcal{X} for suitably small values of μ . In particular, a sufficient upper bound to $|U_j(s)|$ is obtained if, for example, during the transit we have $\Gamma_s \leq (3/2)\Gamma_0$ (see Section 3 for all the details). In Section 3 we prove that, if μ satisfies:

$$\mu < c(1 - \varepsilon)^6 \Gamma_0^{\frac{3}{2}}, \quad (8)$$

where $c > 0$ is a suitable constant independent of $\mu, \varepsilon, \Gamma_0$, then during the transit in the Hill's sphere we have $\Gamma_s \in [\Gamma_0/2, (3/2)\Gamma_0]$, so that the matrix \mathcal{X}_0 is hyperbolic; an additional smallness condition on μ grants that also the matrix \mathcal{X} is hyperbolic. Therefore, we justify the effectiveness of the RFLIs to detect orbits with multiple fast close encounters also for the ER3BP when the parameter μ is small. We also provide numerical demonstrations of the detection of close encounters with regularized Lyapunov indicators.

The paper is structured as follows. In Section 2 we present a step-by-step construction of the regularization, with the final rigorous statement on the projection of the solutions and related proof. Section 3 is dedicated to the discussion of fast close encounters of the ER3BP and specifically we justify (8) as a condition sufficient for the hyperbolicity

of the encounter. Section 4 is dedicated to numerical demonstrations: Section 4.1 describes how to implement the KS regularization scheme with the transformations needed; Section 4.2, after a short description of the considered scenarios, deals with numerical explorations in a neighborhood of P_2 and outlines quantitatively the gain as regards the computational effort; Section 4.3 reports examples of detection of fast close encounters with RFLIs in the ER3BP. Section 5 contains intermediate estimates necessary to prove the statements of Section 3. In Section 6 we draw our conclusions. We include the transformations to pass from the synodic to the inertial reference frame in the Appendix.

2. KS regularization of the ER3BP in the synodic reference frame

As described in Section 1, consider the Hamiltonian (1) of the ER3BP, which is conveniently expressed in a synodic rotating-pulsating Cartesian frame [14] where the bodies P_1, P_2 have coordinates $(-\mu, 0, 0)$, $(1 - \mu, 0, 0)$ respectively.

Let us now introduce a local regularization on the secondary body³ P_2 . Following [3,4] we introduce the KS space map as a projection from a space of redundant variables u_1, u_2, u_3, u_4 to a space of Cartesian variables q_1, q_2, q_3 :

$$\pi: \mathbb{R}^4 \longrightarrow \mathbb{R}^3 \quad (9)$$

$$u = (u_1, u_2, u_3, u_4) \longmapsto \pi(u) = (q_1, q_2, q_3) = q,$$

where

$$(q_1, q_2, q_3, 0) = A(u)u \quad (10)$$

are related to (x, y, z) by

$$(x - 1 + \mu, y, z) = q \quad (11)$$

and

$$A(u) = \begin{pmatrix} u_1 & -u_2 & -u_3 & u_4 \\ u_2 & u_1 & -u_4 & -u_3 \\ u_3 & u_4 & u_1 & u_2 \\ u_4 & -u_3 & u_2 & -u_1 \end{pmatrix} \quad (12)$$

is a matrix that plays a central role in the KS regularization. In particular, $A(u)$ fulfills the two properties: it is a linear homogeneous function of u_1, u_2, u_3, u_4 and satisfies:

$$A(u)A^T(u) = A^T(u)A(u) = \|u\|^2 \mathbb{I}, \quad (13)$$

where \mathbb{I} is the 4-by-4 identity matrix; hence $\|u\|^2 = d_2$.

In this article we exploit directly such transformation in the elliptic framework by adapting the Hamiltonian derivation of the KS regularization developed in [23] for the CR3BP. We prove that a KS regularization with respect to the secondary body P_2 of the ER3BP is represented by the Hamiltonian:

$$\begin{aligned} \mathcal{K}(u, \phi, U, \Phi) &= \frac{1}{8} \|U - b(u)\|^2 \\ &- \frac{1}{1 + \varepsilon \cos \phi} \left[(1 - \mu) \|u\|^2 \left(\frac{1}{\|\pi(u) + (1, 0, 0)\|} + \pi_1(u) \right) + \mu \right. \\ &\left. + \frac{1}{2} \|u\|^2 (\pi_1^2(u) + \pi_2^2(u) - \pi_3^2(u) \varepsilon \cos \phi) + \frac{(1 - \mu)^2}{2} \|u\|^2 \right] + \Phi \|u\|^2, \end{aligned} \quad (14)$$

where $u, U = (U_1, U_2, U_3, U_4)$ are the KS variables and their conjugate momenta and Φ is an action conjugate to ϕ introduced to make

² By 'hyperbolic matrix' we mean that the linear operator defined by the exponential of the matrix is hyperbolic.

³ The local regularization at the primary body P_1 could be introduced following the same scheme. We here focus on the regularization at P_2 which is particularly relevant for applications to the motion of asteroids, comets and space-flight dynamics.

autonomous the problem. The vector $b(u)$ is defined by:

$$b(u) = 2A^T(u)\Lambda A(u)u, \quad \Lambda = \begin{pmatrix} 0 & -1 & 0 & 0 \\ 1 & 0 & 0 & 0 \\ 0 & 0 & 0 & 0 \\ 0 & 0 & 0 & 0 \end{pmatrix}. \quad (15)$$

Specifically we show that, by adopting a fictitious time s as new independent variable, the solutions $(u(s), \phi(s), U(s), \Phi(s))$ of Hamilton equations related to $\mathcal{K}(u, \phi, U, \Phi)$:

$$\frac{du}{ds} = \frac{\partial \mathcal{K}}{\partial U}, \quad \frac{d\phi}{ds} = \frac{\partial \mathcal{K}}{\partial \Phi}, \quad \frac{dU}{ds} = -\frac{\partial \mathcal{K}}{\partial u}, \quad \frac{d\Phi}{ds} = -\frac{\partial \mathcal{K}}{\partial \phi},$$

that, for $s = 0$, satisfy:

- (i) $u(0) \neq 0$,
- (ii) $l(u(0), U(0)) = 0$, with $l(u, U) = u_4 U_1 - u_3 U_2 + u_2 U_3 - u_1 U_4$,
- (iii) $\mathcal{K}(u(0), \phi(0), U(0), \Phi(0)) = 0$, $\phi(0) = f_0$

project (via π , the translation $x \mapsto x + 1 - \mu$ and $df/ds = \|u\|^2 = d_2$), locally to $s = 0$, onto solutions $(x(f), y(f), z(f), p_1(f), p_2(f), p_3(f))$ of Hamilton equations from (1).

2.1. Lagrangian formulation in the rotating-pulsating frame

Let $L(x, y, z, x', y', z', f)$ be the Lagrangian of the spatial ER3BP in the rotating-pulsating frame with explicit dependence on the true anomaly⁴ f (the superscript denotes the derivative with respect to that):

$$L(x, y, z, x', y', z', f) = \frac{1}{2} \left((x')^2 + (y')^2 + (z')^2 \right) + xy' - x'y + \frac{1}{1 + \varepsilon \cos f} \left(\frac{1 - \mu}{d_1} + \frac{\mu}{d_2} + \frac{1}{2} (x^2 + y^2 - z^2 \varepsilon \cos f) \right), \quad (16)$$

where, explicitly,

$$d_1 = \sqrt{(x + \mu)^2 + y^2 + z^2}$$

and

$$d_2 = \sqrt{(x - 1 + \mu)^2 + y^2 + z^2}.$$

The origin of the coordinate axes is now moved to one of the two singular positions and thus, as mentioned above in Section 2, we choose $P_2(x_2, y_2, z_2)$:

$$(x - x_2, y, z) = q. \quad (17)$$

Then (16) becomes:

$$\begin{aligned} \tilde{L}(q, q', f) &= \frac{1}{2} \|q'\|^2 + q' \times (0, 0, 1) \cdot q \\ &+ \frac{1}{1 + \varepsilon \cos f} \left[(1 - \mu) \left(\frac{1}{\|q + (1, 0, 0)\|} + q_1 \right) \right. \\ &\left. + \frac{\mu}{\|q\|} + \frac{1}{2} (q_1^2 + q_2^2 - q_3^2 \varepsilon \cos f) \right], \end{aligned} \quad (18)$$

where the addenda $q' \times (0, 0, 1) \cdot (x_2, 0, 0)$ and $(1 - \mu)^2 / (2(1 + \varepsilon \cos f))$ have been dropped because they do not contribute to the Lagrange equations.

2.2. The space of redundant variables

By following [23] and applying their argument to the elliptic problem, we apply the projection map defined by (10) to the previous

⁴ The change of time from t to f is a classic simplification [14,40], where f is thought taking values in the covering \mathbb{R} of $\mathbb{S}^1 \cong \mathbb{T}$.

Lagrangian \tilde{L} , and we compute the function $\mathcal{L}(u, u', f)$ exploiting the relationship:

$$(q'_1, q'_2, q'_3, 0) = 2A(u)u' - 2(0, 0, 0, l(u, u')),$$

in which

$$l(u, u') = u_4 u'_1 - u_3 u'_2 + u_2 u'_3 - u_1 u'_4 \quad (19)$$

is the bilinear form appearing in the usual KS regularization. We obtain:

$$\begin{aligned} \mathcal{L}(u, u', f) &= \tilde{L} \left(\pi(u), \frac{\partial \pi}{\partial u}(u)u', f \right) = 2\|u\|^2 \|u'\|^2 - 2l^2(u, u') + b(u) \cdot u' \\ &+ \frac{1}{1 + \varepsilon \cos f} \left[(1 - \mu) \left(\frac{1}{\|\pi(u) + (1, 0, 0)\|} + \pi_1(u) \right) \right. \\ &\left. + \frac{\mu}{\|u\|^2} + \frac{1}{2} (\pi_1^2(u) + \pi_2^2(u) - \pi_3^2(u) \varepsilon \cos f) \right], \end{aligned} \quad (20)$$

for $b(u)$ expressed as in (15).

The first task consists in proving the specific invariance of Lagrange equations under the transformation at issue. In practice, the solutions of Lagrange equations for $\mathcal{L}(u, u', f)$, which we write using the operator notation:

$$[\mathcal{L}]_i(u, u', u'', f) = \frac{d}{df} \frac{\partial \mathcal{L}}{\partial u'_i} - \frac{\partial \mathcal{L}}{\partial u_i} = 0, \quad \forall i = 1, 2, 3, 4, \quad (21)$$

have to be compared with the solutions of Lagrange equations for $\tilde{L}(q, q', f)$, denoted by:

$$\langle \tilde{L} \rangle_j(q, q', q'', f) = \frac{d}{df} \frac{\partial \tilde{L}}{\partial q'_j} - \frac{\partial \tilde{L}}{\partial q_j} = 0, \quad \forall j = 1, 2, 3. \quad (22)$$

With the following statement it turns out that this requirement is fulfilled as soon as the solution $u(f) \neq 0$ for all $f \in \mathbb{T}$.

Proposition 1. *If $u(f)$ is a solution of Lagrange equations associated to $\mathcal{L}(u, u', f)$ with initial condition $u(0) \neq 0$, then $q(f) = \pi(u(f))$ is a solution of Lagrange equations associated to $\tilde{L}(q, q', f)$ as soon as $u(f) \neq 0$.*

Proof. For any smooth curve $u(f)$, reminding that:

$$\mathcal{L}(u, u', f) = \tilde{L} \left(\pi(u), \frac{\partial \pi}{\partial u}(u)u', f \right),$$

as well as

$$\frac{\partial q'_j}{\partial u'_i} = \frac{\partial \pi}{\partial u_i},$$

one gets from the chain rule:

$$\frac{\partial \mathcal{L}}{\partial u'_i} = \sum_{j=1}^3 \frac{\partial \tilde{L}}{\partial q'_j} \frac{\partial q'_j}{\partial u'_i} = \sum_{j=1}^3 \frac{\partial \tilde{L}}{\partial q'_j} \frac{\partial \pi_j}{\partial u_i}$$

and

$$\begin{aligned} \frac{d}{df} \frac{\partial \mathcal{L}}{\partial u'_i} &= \sum_{j=1}^3 \frac{d}{df} \frac{\partial \tilde{L}}{\partial q'_j} \frac{\partial \pi_j}{\partial u_i} + \sum_{j=1}^3 \frac{\partial \tilde{L}}{\partial q'_j} \frac{d}{df} \frac{\partial \pi_j}{\partial u_i} \\ &= \sum_{j=1}^3 \frac{d}{df} \frac{\partial \tilde{L}}{\partial q'_j} \frac{\partial \pi_j}{\partial u_i} + \sum_{j=1}^3 \frac{\partial \tilde{L}}{\partial q'_j} \sum_{k=1}^4 \frac{\partial^2 \pi_j}{\partial u_i \partial u_k} u'_k, \end{aligned}$$

$$\frac{\partial \mathcal{L}}{\partial u_i} = \sum_{j=1}^3 \frac{\partial \tilde{L}}{\partial q_j} \frac{\partial \pi_j}{\partial u_i} + \sum_{j=1}^3 \frac{\partial \tilde{L}}{\partial q'_j} \sum_{k=1}^4 \frac{\partial^2 \pi_j}{\partial u_i \partial u_k} u'_k,$$

for $i = 1, 2, 3, 4$. As a consequence we have:

$$\begin{aligned} [\mathcal{L}](u(f), u'(f), u''(f), f) \\ = \left(\frac{\partial \pi}{\partial u}(u(f)) \right)^T \langle \tilde{L} \rangle \left(\pi(u(f)), \frac{d}{df} \pi(u(f)), \frac{d^2}{df^2} \pi(u(f)), f \right) \end{aligned}$$

where $[\mathcal{L}] \in \mathbb{R}^4$, $\langle \tilde{L} \rangle \in \mathbb{R}^3$ are the vectors of components respectively $[\mathcal{L}]_i$, $\langle \tilde{L} \rangle_j$.

Since by assumption $[\mathcal{L}]_i(u(f), u'(f), u''(f), f) = 0$, the vector

$$\langle \tilde{L} \rangle \left(\pi(u(f)), \frac{d}{df} \pi(u(f)), \frac{d^2}{df^2} \pi(u(f)), f \right)$$

is for any f in the kernel of the matrix $\left(\frac{\partial \pi}{\partial u}(u(f))\right)^T$. We claim that the kernel of $\left(\frac{\partial \pi}{\partial u}(u(f))\right)^T$ contains only $(0, 0, 0)$ if $u \neq 0$. In fact, an element (α, β, η) is in the kernel of $\left(\frac{\partial \pi}{\partial u}(u(f))\right)^T$ if and only if its components satisfy the system:

$$\begin{cases} u_1\alpha + u_2\beta + u_3\eta = 0 \\ -u_2\alpha + u_1\beta + u_4\eta = 0 \\ -u_3\alpha - u_4\beta + u_1\eta = 0 \\ u_4\alpha - u_3\beta + u_2\eta = 0 \end{cases},$$

which admits the unique solution $\alpha = \beta = \eta = 0$ as long as at least one of the components of u is different from zero.

This implies $\langle \tilde{L} \rangle \left(\pi(u(f)), \frac{d}{df} \pi(u(f)), \frac{d^2}{df^2} \pi(u(f)), f \right) = 0$ and $q(f) = \pi(u(f))$ is a solution of the Lagrange equations of \tilde{L} . \square

The modified Lagrangian

The second matter to tackle regards the Legendre transform (necessary to deduce in Section 2.3 the corresponding transformed Hamiltonian and then proceed with the development):

$$\frac{\partial \mathcal{L}}{\partial u'} = \left(\frac{\partial \mathcal{L}}{\partial u'_1}, \frac{\partial \mathcal{L}}{\partial u'_2}, \frac{\partial \mathcal{L}}{\partial u'_3}, \frac{\partial \mathcal{L}}{\partial u'_4} \right) = 4\|u\|^2 u' - 4(\Omega u \cdot u') \Omega u + b(u), \quad (23)$$

where

$$\Omega = \begin{pmatrix} 0 & 0 & 0 & 1 \\ 0 & 0 & -1 & 0 \\ 0 & 1 & 0 & 0 \\ -1 & 0 & 0 & 0 \end{pmatrix} \quad (24)$$

is an ad hoc permutation matrix coming from the bilinear form term $(l(u, u') = \Omega u \cdot u')$, which is not invertible with respect to the generalized velocities, because the Hessian matrix

$$\mathcal{H}_{u'} = \left(\frac{\partial^2 \mathcal{L}}{\partial u'_i \partial u'_j} \right), \quad i, j \in \{1, 2, 3, 4\}, \quad (25)$$

is identically singular, indeed $\det \mathcal{H}_{u'} = 0$. To overcome the degeneracy we proceed as in [23]: it is profitable to change the Lagrangian just by adding two times the square of the bilinear form (so that $-2l^2$ vanishes): such artifice precisely allows to restore the invertibility, thereby:

$$\begin{aligned} \mathcal{L}(u, u', f) &= \mathcal{L}(u, u', f) + 2l^2(u, u') = 2\|u\|^2 \|u'\|^2 + b(u) \cdot u' \\ &+ \frac{1}{1 + \varepsilon \cos f} \left[(1 - \mu) \left(\frac{1}{\|\pi(u) + (1, 0, 0)\|} + \pi_1(u) \right) \right. \\ &\left. + \frac{\mu}{\|u\|^2} + \frac{1}{2} (\pi_1^2(u) + \pi_2^2(u) - \pi_3^2(u) \varepsilon \cos f) \right] \end{aligned} \quad (26)$$

is the modified Lagrangian and in fact, introducing the KS momenta $U = (U_1, U_2, U_3, U_4)$ conjugate to $u = (u_1, u_2, u_3, u_4)$, the relationship

$$U = \frac{\partial \mathcal{L}}{\partial u'}(u, u') = 4\|u\|^2 u' + b(u) \quad (27)$$

is non-degenerate (thus invertible) in u' for $u \neq 0$.

Rotational invariance of the modified Lagrangian

The sum of the quadratic expression $2l^2(u, u')$ of course alters $\mathcal{L}(u, u', f)$ and again one has to make sure that such action is legitimized under appropriate conditions (until now $u(f) \neq 0$ always). Let then the investigation begin by realizing the well known remarkable symmetry property of the KS transformation.

Proposition 2. *The modified Lagrangian $\mathcal{L}(u, u', f)$ is invariant under the one-parameter family of transformations involving the redundant coordinates:*

$$S_\theta : \mathbb{R}^4 \longrightarrow \mathbb{R}^4 \\ u \longmapsto S_\theta u, \quad (28)$$

where $S_\theta \in SO(4)$ is the four-dimensional rotation matrix

$$S_\theta = \begin{pmatrix} \cos \theta & 0 & 0 & -\sin \theta \\ 0 & \cos \theta & \sin \theta & 0 \\ 0 & -\sin \theta & \cos \theta & 0 \\ \sin \theta & 0 & 0 & \cos \theta \end{pmatrix}, \quad (29)$$

whose orbits define the fibers of the projection π , i.e., $\pi(S_\theta u) = \pi(u)$ for all $\theta \in \mathbb{T}$. More precisely:

$$\mathcal{L}(S_\theta u, S_\theta u', f) = \mathcal{L}(u, u', f). \quad (30)$$

Proof. This is a property of the KS transformation, which is the same for the CR3BP and for the ER3BP. Thus, for the proof we refer to [23], Section 2. \square

This fact implies that there exists, by Noether's theorem, a conserved quantity:

$$J(u, u') = \frac{\partial \mathcal{L}}{\partial u'} \cdot \frac{d}{d\theta} S_\theta u \Big|_{\theta=0} = -4\|u\|^2 l(u, u') - b(u) \cdot \Omega u = -4\|u\|^2 l(u, u')$$

which is an autonomous first integral for the Lagrangian \mathcal{L} . For convenience the final constant of motion is given by:

$$J(u, u') = \|u\|^2 l(u, u'). \quad (31)$$

If the bilinear form is cleverly zeroed out at $f = 0$ (by proper initial conditions), it will keep taking zero value for further f (since we only consider time intervals such that $\|u\| \neq 0$), so the extra factor $2l^2$ would become a vanishing contribution to the Lagrange equations.

According to such idea, the equation $l(u, u') = 0$ becomes a constraint to be respected along the motion. We prove now that the Lagrange equations associated to \mathcal{L} have the same solutions of the Lagrange equations associated to \mathcal{L} .

Proposition 3. *If $u(f)$ is a solution of the Lagrange equations of $\mathcal{L}(u, u', f)$ with initial data $u(0), u'(0)$ satisfying $u(0) \neq 0$ and $l(u(0), u'(0)) = 0$, then it is also a solution of the Lagrange equations of $\mathcal{L}(u, u', f)$ as long as $u(f) \neq 0$.*

Proof. Consider a solution $u(f)$ of the \mathcal{L} -equations with $u(0) \neq 0$ and $l(u(0), u'(0)) = 0$. As long as $u(f) \neq 0$, by (31), $l(u(f), u'(f)) = 0$. Moreover:

$$\frac{d}{df} l(u(f), u'(f)) = l(u'(f), u'(f)) + l(u(f), u''(f)) = l(u(f), u''(f)).$$

Now $u(f)$ solves the Lagrange equations for \mathcal{L} too, in fact, referring to the previous notation (21), for any $i = 1, 2, 3, 4$:

$$\begin{aligned} [\mathcal{L}]_i &= [\mathcal{L} - 2l^2]_i = [\mathcal{L}]_i - 2 \left(\frac{d}{df} \frac{\partial}{\partial u'_i} l^2(u, u') - \frac{\partial}{\partial u_i} l^2(u, u') \right) \\ &= [\mathcal{L}]_i - 4 \left[\frac{d}{df} \left(l(u, u') \frac{\partial}{\partial u'_i} l(u, u') \right) - l(u, u') \frac{\partial}{\partial u_i} l(u, u') \right] \end{aligned}$$

and when evaluated along the curve $u(f)$:

$$\begin{aligned} [\mathcal{L}]_i(u(f), u'(f), u''(f), f) &= [\mathcal{L}]_i(u(f), u'(f), u''(f), f) \\ &- 4 \left(l(u(f), u''(f)) \frac{\partial}{\partial u'_i} l(u(f), u'(f)) + l(u(f), u'(f)) \frac{d}{df} \frac{\partial}{\partial u'_i} l(u(f), u'(f)) \right. \\ &\left. - l(u(f), u'(f)) \frac{\partial}{\partial u_i} l(u(f), u'(f)) \right) = 0, \end{aligned}$$

owing to $l(u(f), u''(f)) = l(u(f), u'(f)) = 0$. \square

2.3. The regularized Hamiltonian

The corresponding singular Hamiltonian enters now by performing the Legendre transform:

$$\mathcal{H}(u, U, f) = U \cdot g(u, U) - \mathcal{L}(u, g(u, U), f), \quad (32)$$

where

$$u' = g(u, U) = \frac{U - b(u)}{4\|u\|^2}$$

is the inverse of U with respect to u' ; more explicitly we have:

$$\begin{aligned} \mathcal{H}(u, U, f) &= \frac{1}{8\|u\|^2} \|U - b(u)\|^2 \\ &- \frac{1}{1 + \varepsilon \cos f} \left[(1 - \mu) \left(\frac{1}{\|\pi(u) + (1, 0, 0)\|} + \pi_1(u) \right) \right. \\ &\left. + \frac{\mu}{\|u\|^2} + \frac{1}{2} (\pi_1(u)^2 + \pi_2(u)^2 - \pi_3(u)^2 \varepsilon \cos f) \right] \end{aligned} \quad (33)$$

and the bilinear equality $l(u, u') = 0$ straightforwardly translates in the Hamiltonian formalism as $l(u, U) = 0$ for $u \neq 0$, because

$$l(u, u') = l(u, g(u, U)) = \frac{1}{4\|u\|^2} l(u, U) - \frac{1}{4\|u\|^2} l(u, b(u)),$$

but $l(u, b(u)) = \Omega u \cdot b(u) = 0$ identically, hence we have $l(u, u') = 0$ if and only if $l(u, U) = 0$.

With all this in hands it is useful to work with an autonomous extension of the transformed Hamiltonian \mathcal{H} . So we append one more degree of freedom to form the extended phase-space $T^*((\mathbb{R}^4 \setminus \mathcal{C}) \times \mathbb{T})$, where

$$\mathcal{C} = \{(0, 0, 0, 0)\} \cup \{(0, u_2, u_3, 0) : u_2^2 + u_3^2 = 1\} \quad (34)$$

is the collision set in KS coordinates, with the extra couple of variables $(\phi, \Phi) \in \mathbb{T} \times \mathbb{R}$ and standard symplectic form $\sum_{i=1}^4 du_i \wedge dU_i + d\phi \wedge d\Phi$, in such a way to build the autonomous transformed Hamiltonian:

$$\widehat{\mathcal{H}}(u, \phi, U, \Phi) = \mathcal{H}(u, U, \phi) + \Phi, \quad (35)$$

and consider the solutions $u(f), \phi(f), U(f), \Phi(f)$ of the Hamilton equations of (35) such that, for given initial value f_0 of the true anomaly, satisfy:

$$u(f_0) = u_0, \quad \phi(f_0) = f_0, \quad U(f_0) = U_0, \quad \Phi(f_0) = -\mathcal{H}(u_0, U_0, f_0).$$

At this point we perform a rescaling similar to the one in the Levi-Civita regularization, and define the regularized Hamiltonian:

$$\begin{aligned} \mathcal{K}(u, \phi, U, \Phi) &= \|u\|^2 \widehat{\mathcal{H}}(u, \phi, U, \Phi) = \frac{1}{8} \|U - b(u)\|^2 \\ &- \frac{1}{1 + \varepsilon \cos \phi} \left[(1 - \mu) \|u\|^2 \left(\frac{1}{\|\pi(u) + (1, 0, 0)\|} + \pi_1(u) \right) + \mu \right. \\ &\left. + \frac{1}{2} \|u\|^2 (\pi_1(u)^2 + \pi_2(u)^2 - \pi_3(u)^2 \varepsilon \cos \phi) + \frac{(1 - \mu)^2}{2} \|u\|^2 \right] + \Phi \|u\|^2. \end{aligned} \quad (36)$$

Remark 1.

- For $\varepsilon = 0$, the action Φ is a constant of motion and the Hamiltonian (36) is identical to the KS Hamiltonian of the CR3BP, as represented in [23] with $\Phi = -E$.
- $\mathcal{K}(u, \phi, U, \Phi)$ is invariant under the same one-parameter family of transformations defined by (28) and (29), hence $\mathcal{J}(u, g(u, U)) = l(u, U)$ is a first integral also for the Hamilton equations of $\mathcal{K}(u, \phi, U, \Phi)$.
- Hamiltonian (36) is regular at $u = 0$.

2.4. Projection of the solutions of the regularized Hamiltonian

Let us prove that the solutions of the Hamilton equations of the regularized Hamiltonian (36) project on the Hamilton solutions of the

Hamiltonian (1) of the ER3BP. Similarly to the classic LC and KS techniques we need an independent variable redefinition, which for the ER3BP is obtained by introducing the fictitious true anomaly s such that:

$$s'(f) = \frac{1}{\|u(f)\|^2}, \quad s(f_0) = 0, \quad (37)$$

whose inverse is precisely $\partial \mathcal{K} / \partial \Phi$. Thereby we state our result.

Theorem 1. *The solutions $(u(s), \phi(s), U(s), \Phi(s))$ of Hamilton equations related to $\mathcal{K}(u, \phi, U, \Phi)$ with initial conditions satisfying:*

- (i) $u(0) \neq 0$,
- (ii) $l(u(0), U(0)) = 0$,
- (iii) $\mathcal{K}(u(0), \phi(0), U(0), \Phi(0)) = 0, \phi(0) = f_0$,

project, for s in a neighborhood of $s = 0$, via the true anomaly reparametrization:

$$f(s) = f_0 + \int_0^s \|u(\sigma)\|^2 d\sigma, \quad (38)$$

the transformation (10) and the translation (11), onto solutions $(x(f), y(f), z(f), p_1(f), p_2(f), p_3(f))$ of the Hamilton equations of Hamiltonian (1).

Proof. In light of what already derived in the previous Sections, we only need to prove the equivalence between the solutions associated to the transformed $\widehat{\mathcal{H}}$ and the regularized \mathcal{K} . Given the initial conditions u_0, U_0, f_0 , let us consider the solution $(\tilde{u}(s), \tilde{\phi}(s), \tilde{U}(s), \tilde{\Phi}(s))$ of the Hamilton equations of \mathcal{K} with:

$$\tilde{u}(0) = u_0, \quad \tilde{U}(0) = U_0, \quad \tilde{\phi}(0) = f_0, \quad \tilde{\Phi}(0) = -\mathcal{H}(u_0, U_0, f_0),$$

and s in a neighborhood of $s = 0$ such that $\|\tilde{u}(s)\| > 0$; in particular we have:

$$\mathcal{K}(\tilde{u}(s), \tilde{\phi}(s), \tilde{U}(s), \tilde{\Phi}(s)) = 0$$

for all s . Next, consider:

$$f(s) = f_0 + \int_0^s \|\tilde{u}(\sigma)\|^2 d\sigma,$$

which is invertible (since in the neighborhood of $s = 0$ we have $\|\tilde{u}(s)\| > 0$), and $(u(f), \phi(f), U(f), \Phi(f))$ defined by:

$$u(f) = \tilde{u}(s(f)), \quad U(f) = \tilde{U}(s(f)), \quad \phi(f) = \tilde{\phi}(s(f)), \quad \Phi(f) = \tilde{\Phi}(s(f)).$$

We claim that $(u(f), \phi(f), U(f), \Phi(f))$ are the solutions of the Hamilton equations of $\widehat{\mathcal{H}}$ with initial conditions $(u(f_0), \phi(f_0), U(f_0), \Phi(f_0)) = (u_0, f_0, U_0, -\mathcal{H}(u_0, U_0, f_0))$. In fact, we have:

$$\begin{aligned} \frac{du_i}{df} &= \frac{ds}{df} \frac{d\tilde{u}_i}{ds} \Big|_{s=s(f)} = \frac{1}{\|\tilde{u}(s(f))\|^2} \left[\frac{\partial}{\partial U_i} \left(\|u\|^2 \widehat{\mathcal{H}} \right) \right] \Big|_{(u, \phi, \Phi) = (\tilde{u}(s), \tilde{\phi}(s), \tilde{\Phi}(s)), s=s(f)} \\ &= \left[\frac{\partial}{\partial U_i} \widehat{\mathcal{H}} \right] (\tilde{u}(s(f)), \tilde{\phi}(s(f)), \tilde{U}(s(f)), \tilde{\Phi}(s(f))) \\ &= \left[\frac{\partial}{\partial U_i} \widehat{\mathcal{H}} \right] (u(f), \phi(f), U(f), \Phi(f)), \end{aligned}$$

as well as:

$$\begin{aligned} \frac{d\phi}{df} &= \frac{ds}{df} \frac{d\tilde{\phi}}{ds} \Big|_{s=s(f)} = \frac{1}{\|\tilde{u}(s(f))\|^2} \left[\frac{\partial}{\partial \Phi} \left(\|u\|^2 \widehat{\mathcal{H}} \right) \right] \Big|_{(u, \phi, \Phi) = (\tilde{u}(s), \tilde{\phi}(s), \tilde{\Phi}(s)), s=s(f)} \\ &= \frac{\partial \widehat{\mathcal{H}}}{\partial \Phi} = 1 \end{aligned}$$

and:

$$\frac{dU_i}{df} = \frac{ds}{df} \frac{d\tilde{U}_i}{ds} \Big|_{s=s(f)} = -\frac{1}{\|\tilde{u}(s(f))\|^2} \left[\frac{\partial}{\partial u_i} \left(\|u\|^2 \widehat{\mathcal{H}} \right) \right] \Big|_{(u, \phi, \Phi) = (\tilde{u}(s), \tilde{\phi}(s), \tilde{\Phi}(s)), s=s(f)}$$

$$\begin{aligned}
&= - \left[\frac{\partial}{\partial u_i} \widehat{\mathcal{K}} \right] (\tilde{u}(s(f)), \tilde{\phi}(s(f)), \tilde{U}(s(f)), \tilde{\Phi}(s(f))) \\
&= - \left[\frac{\partial}{\partial u_i} \widehat{\mathcal{K}} \right] (u(f), \phi(f), U(f), \Phi(f)),
\end{aligned}$$

where to obtain the second equality we used $\widehat{\mathcal{K}}(\tilde{u}(s), \tilde{\phi}(s), \tilde{U}(s), \tilde{\Phi}(s)) = 0$. Finally, we also have:

$$\begin{aligned}
&\frac{d\Phi}{df} \\
&= \frac{ds}{df} \frac{d\tilde{\Phi}}{ds} \Big|_{s=s(f)} = - \frac{1}{\|\tilde{u}(s(f))\|^2} \left[\frac{\partial}{\partial \phi} \left(\|\tilde{u}\|^2 \widehat{\mathcal{K}} \right) \right] \Big|_{(u, U, \phi, \Phi) = (\tilde{u}(s), \tilde{\phi}(s), \tilde{U}(s), \tilde{\Phi}(s)), s=s(f)} \\
&= - \left[\frac{\partial}{\partial \phi} \widehat{\mathcal{K}} \right] (\tilde{u}(s(f)), \tilde{\phi}(s(f)), \tilde{U}(s(f)), \tilde{\Phi}(s(f))) \\
&= - \left[\frac{\partial}{\partial \phi} \widehat{\mathcal{K}} \right] (u(f), \phi(f), U(f), \Phi(f)). \quad \square
\end{aligned}$$

Remark 2. The reason for the success of this Hamiltonian regularization is, as for the spatial CR3BP, the possibility to exploit the symmetry presented in Proposition 2 in the framework of symplectic reductions (see [41–44]) in the 10-dimensional phase-space (u, ϕ, U, Φ) .

3. Fast close encounters in the ER3BP

In order to discuss a sufficient condition to have hyperbolic close encounters in the ER3BP, we first represent the regularized Hamiltonian (14) in the form:

$$\mathcal{K} = \frac{1}{8} \|U - b(u)\|^2 - \|u\|^2 \left[-\Phi + \frac{3 - 4\mu + \mu^2}{2(1 + \varepsilon \cos \phi)} \right] - \frac{\mu}{1 + \varepsilon \cos \phi} + \mathcal{R}_6(u, \phi), \quad (39)$$

where

$$\begin{aligned}
\mathcal{R}_6 &= - \frac{1}{1 + \varepsilon \cos \phi} \left[(1 - \mu) \|u\|^2 \left(\frac{1}{\|\pi(u) + (1, 0, 0)\|} + \pi_1(u) - 1 \right) \right. \\
&\quad \left. + \frac{1}{2} \|u\|^2 (\pi_1^2(u) + \pi_2^2(u) - \pi_3^2(u) \varepsilon \cos \phi) \right] \quad (40)
\end{aligned}$$

has Taylor expansion with respect to the variables u starting at order 6. In fact, the Taylor expansion of $1/\|\pi + (1, 0, 0)\| + \pi_1 - 1$ with respect to π_1, π_2, π_3 starts at order 2, and the π_j are quadratic functions of the u_i . Using standard estimates (see item (i) below), we provide upper bounds to the remainder \mathcal{R}_6 and its derivatives in the ball:

$$B(\mu^{\frac{1}{6}}) = \{u \in \mathbb{R}^4 : \|u\| < \mu^{\frac{1}{6}}\}, \quad (41)$$

projecting to the ball in the Cartesian space:

$$B(\mu^{\frac{1}{3}}) = \{q \in \mathbb{R}^3 : \|q\| < \mu^{\frac{1}{3}}\}. \quad (42)$$

We will refer to both spheres (41) and (42) as the Hill's sphere (notice that the terminology is different from the conventional one by a numerical factor in the radius of the sphere).

As explained in Section 1, by comparing the regularized Hamiltonian (39) of the ER3BP with the regularized Hamiltonian (3) of the CR3BP, we notice the analogy between the coefficient $\Gamma(\phi, \Phi)$ (defined in (5)) and the coefficient γ (defined in (2)) characterizing the hyperbolicity of the encounters of the CR3BP. The main important difference is that while γ is a parameter, Γ is a function of the variables ϕ, Φ , and therefore is not constant along the solutions $(u(s), \phi(s), U(s), \Phi(s))$ of the Hamilton equations of \mathcal{K} .

Let us consider solutions $q(f)$ of the ER3BP transiting through the Hill's sphere of the secondary body P_2 in the f -interval $[f_1, f_2]$, i.e., $\|q(f_1)\| = \|q(f_2)\| = \mu^{1/3}$ and $0 < \|q(f)\| < \mu^{1/3}$ for all $f \in (f_1, f_2)$, and denote by $(u(s), \phi(s), U(s), \Phi(s))$ a solution of the Hamilton equations of the regularized Hamiltonian \mathcal{K} satisfying the hypotheses of Section 2.4 such that $\pi(u(s)) = q(f(s))$ for all $s \in [s_1, s_2]$ (s_1, s_2 corresponding to f_1, f_2).

In this Section we provide a sufficient condition on the transit which

rules out the possibility that a motion enters the Hill's sphere with a positive value $\Gamma_0 := \Gamma_{s_1}$ and during the transit the values of Γ becomes negative. As a matter of fact, we first prove that the function

$$\Gamma_s := \Gamma(\phi(s), \Phi(s)) \quad (43)$$

has variations which are slow, for small values of μ during the transit, i.e., for all $s \in [s_1, s_2]$ (see item (ii) below).

Then we prove that, in analogy with the CR3BP, the value Γ_0 characterizes the velocity of the encounter.

In the specific case of the ER3BP, we show that a smallness condition on μ grants that Γ_s remains bounded in the interval $[\Gamma_0/2, (3/2)\Gamma_0]$ during the close encounter (see items (iii), (iv), (v) below).

This is sufficient to grant the hyperbolicity of the matrices \mathcal{X}_0 and \mathcal{X} (see item (vi)).

Below, we denote by μ_0 , by $c_1, c_2, \dots > 0$ and by $\gamma_1, \gamma_2, \dots > 0$ constants which are independent of μ and ε , as well as on the parameter Γ_0 which will be later introduced again to characterize each close encounter.

(i) There exist constants $c_1, c_2, c_3, c_4 > 0$ and $\mu_0 \in (0, 1/10)$ such that, for any $\mu \leq \mu_0$, $\varepsilon \in (0, 1)$, $u \in B(\mu_0^{\frac{1}{6}})$ and $\phi \in [0, 2\pi]$, we have:

$$|\mathcal{R}_6(u, \phi)| \leq \frac{c_1}{1 - \varepsilon} \|u\|^6, \quad (44)$$

$$\|b(u)\| \leq c_2 \|u\|^3, \quad (45)$$

$$\sum_i \left| \sum_j u_j \left(\frac{\partial b_i}{\partial u_j} - \frac{\partial b_j}{\partial u_i} \right) \right| \leq c_3 \|u\|^3, \quad (46)$$

$$\left| \sum_i u_i \frac{\partial \mathcal{R}_6}{\partial u_i} \right| \leq \frac{c_4}{1 - \varepsilon} \|u\|^6. \quad (47)$$

The proof is reported in Section 5.1.

(ii) If $\mu \leq \mu_0$, there exists a constant $c_5 > 0$ such that, during the transit in the Hill's sphere, the variation of the function Γ_s in (43) satisfies:

$$\left| \frac{d\Gamma_s}{ds} \right| \leq c_5 \frac{\varepsilon \mu}{(1 - \varepsilon)^2}. \quad (48)$$

The proof is reported in Section 5.2.

A direct consequence of (48) is: by considering transits with $\Gamma_0 := \Gamma_{s_1} > 0$ and proper time intervals $\Delta s > 0$ satisfying:

$$\Delta s \frac{\varepsilon \mu}{(1 - \varepsilon)^2} \leq \frac{\Gamma_0}{2c_5}, \quad (49)$$

for all $s \in [s_1, s_1 + \Delta s] \cap [s_1, s_2]$ we have $\Gamma_s \in [\Gamma_0/2, 3\Gamma_0/2]$; in particular since $\Gamma_s \geq \Gamma_0/2 > 0$, the matrix \mathcal{X}_0 is hyperbolic.

(iii) $\|U(s)\|, \|u(s)\|$ are bounded by quantities which, for $s \in [s_1, s_1 + \Delta s] \cap [s_1, s_2]$, are small with $\mu^{\frac{1}{6}}$. Indeed, for all $s \in [s_1, s_1 + \Delta s] \cap [s_1, s_2]$, using $\mathcal{K}(u(s), \phi(s), U(s), \Phi(s)) = 0$ and (44), we obtain from (39):

$$\frac{1}{8} \|U - b(u)\|^2 = \Gamma_s \|u\|^2 + \frac{\mu}{1 + \varepsilon \cos \phi} - \mathcal{R}_6(u, \phi) \leq \frac{3}{2} \Gamma_0 \|u\|^2 + \frac{\mu}{1 - \varepsilon} + \frac{c_1}{1 - \varepsilon} \|u\|^6$$

and therefore there exists $c_6 > 0$ such that:

$$\|U - b(u)\| \leq c_6 \sqrt{\Gamma_0 \|u\|^2 + \frac{\mu}{1 - \varepsilon}}; \quad (50)$$

by the triangle inequality $\|U\| \leq \|U - b\| + \|b\|$, thus, using (45):

$$\|U\| \leq c_6 \sqrt{\Gamma_0 \|u\|^2 + \frac{\mu}{1 - \varepsilon}} + c_2 \|u\|^3.$$

(iv) It remains to show that, with a suitable smallness condition on μ , each transit in the Hill's sphere with $\Gamma_0 > 0$ occurs in proper time intervals Δs satisfying (49). First, we prove that there exists $c_7 > 0$ (independent on $\mu, \varepsilon, \Gamma_0$) such that if μ satisfies:

$$\mu \leq c_7 (1 - \varepsilon)^2 \Gamma_0^{\frac{3}{2}} \quad (51)$$

and Δs satisfies (49), for all $s \in [s_1, s_1 + \Delta s] \cap [s_1, s_2]$ we have:

$$\frac{d^2 \rho}{ds^2} \geq \frac{\Gamma_0}{2} \rho + \frac{\mu}{1 + \epsilon}, \quad (52)$$

where $\rho(s) := \|u(s)\|^2$ (the proof is reported in Section 5.3).

(v) Finally, we prove in Section 5.4 that if μ satisfies the inequality:

$$\mu < c(1 - \epsilon)^6 \Gamma_0^{\frac{3}{2}} \quad (53)$$

with suitable $c > 0$, the motion exits from the Hill's sphere within a proper time interval satisfying (49).

(vi) Therefore, we have proved that if μ satisfies a smallness condition, the matrix \mathcal{X}_0 is hyperbolic during the transit in the Hill's sphere. Moreover, if the Hill's radius is suitably small (the smallness condition depending possibly on Γ_0), which is obtained by introducing another smallness condition on μ , and since hyperbolicity is persistent under perturbations, then also the matrix \mathcal{X} remains hyperbolic during the transit in the Hill's sphere.

4. Implementation of the KS algorithm and numerical demonstrations

4.1. Implementation procedure of the KS algorithm

We turn the theory developed in Section 2 into an algorithmic procedure, mainly for numerical integration purposes. We detail each step according to the following roadmap to conduct the regularization schematically, from initialization to back-transformation to the original Cartesian solutions.

- (i) **Cartesian initial conditions.** Given an initial Cartesian datum $(x_0, y_0, z_0, p_{1,0}, p_{2,0}, p_{3,0})$ at $f = f_0$, define the values of Φ_0 and ϕ_0 by:

$$\Phi_0 = -\mathcal{H}(x_0, y_0, z_0, p_{1,0}, p_{2,0}, p_{3,0}, f_0), \quad \phi_0 = f_0,$$

where \mathcal{H} is the Hamiltonian in (1). The vector:

$$(x_0, y_0, z_0, \phi_0, p_{1,0}, p_{2,0}, p_{3,0}, \Phi_0)$$

is therefore the initial datum in the Cartesian extended phase-space.

- (ii) **KS-transformed initial conditions.** The correspondence between

$$(u_0, \phi_0, U_0, \Phi_0) :=$$

$$(u_1(0), u_2(0), u_3(0), u_4(0), \phi(0), U_1(0), U_2(0), U_3(0), U_4(0), \Phi(0))$$

and

$$(x(f_0), y(f_0), z(f_0), \phi(f_0), p_1(f_0), p_2(f_0), p_3(f_0), \Phi(f_0))$$

is clearly not one-to-one, therefore below we provide an algorithm to produce initial conditions in the space of the KS variables which project to the initial conditions in the Cartesian phase-space. In order to close the problem, we first consider the local pre-images of the map $\pi(u)$:

$$\begin{aligned} \pi_-^{-1}(q) &= \left(\frac{q_2}{\sqrt{2(d-q_1)}}, \sqrt{\frac{d-q_1}{2}}, 0, \frac{q_3}{\sqrt{2(d-q_1)}} \right) \\ \pi_+^{-1}(q) &= \left(\sqrt{\frac{d+q_1}{2}}, \frac{q_2}{\sqrt{2(d+q_1)}}, \frac{q_3}{\sqrt{2(d+q_1)}}, 0 \right) \end{aligned} \quad (54)$$

with $d = d_2 = \sqrt{q_1^2 + q_2^2 + q_3^2}$. We remark that the maps (54) correspond to the set of formulae right before Equation (8) in [45] with a small caveat on the domain of definition (in the reference, the whole left or right hemi-space of $\mathbb{R}^3 \setminus \{q_1 < 0\}$ or $\{q_1 \geq 0\}$). These local charts can be used interchangeably to compute the KS-transformed initial conditions $(u_0, \phi_0, U_0, \Phi_0)$,

except when $q_2(f_0) = q_3(f_0) = 0$, where the choice $q_1(f_0) = x_0 - 1 + \mu < 0$ or ≥ 0 forces to stick either to π_-^{-1} or π_+^{-1} , respectively, and consequently to extensions $\bar{\pi}_-^{-1}$ or $\bar{\pi}_+^{-1}$ to include the initial conjugate momenta (see below). As in [45], a straightforward possibility consists in setting directly an if-condition on x_0 :

$$\begin{aligned} \text{if } x_0 < 1 - \mu & \quad \text{if } x_0 \geq 1 - \mu \\ u_{1,0} &= \frac{y_0}{\sqrt{2(d-x_0+1-\mu)}} & u_{1,0} &= \sqrt{\frac{d+x_0-1+\mu}{2}} \\ u_{2,0} &= \sqrt{\frac{d-x_0+1-\mu}{2}} & u_{2,0} &= \frac{y_0}{\sqrt{2(d+x_0-1+\mu)}} \\ u_{3,0} &= 0 & u_{3,0} &= \frac{z_0}{\sqrt{2(d+x_0-1+\mu)}} \\ u_{4,0} &= \frac{z_0}{\sqrt{2(d-x_0+1-\mu)}} & u_{4,0} &= 0 \end{aligned} \quad (55)$$

Next, the local pre-images π_-^{-1} , π_+^{-1} are extended to local pre-images of the phase-space:

$$\begin{aligned} \bar{\pi}_-^{-1} : T^*(\mathbb{R}^3 \setminus \{(q_1, 0, 0) : q_1 \geq 0\}) \times \mathbb{T} & \longrightarrow T^*(\mathbb{R}^4 \setminus \mathcal{E}) \times \mathbb{T} \cap \{l = 0\} \\ \bar{\pi}_+^{-1} : T^*(\mathbb{R}^3 \setminus \{(q_1, 0, 0) : q_1 < 0\}) \times \mathbb{T} & \longrightarrow T^*(\mathbb{R}^4 \setminus \mathcal{E}) \times \mathbb{T} \cap \{l = 0\} \end{aligned} \quad (56)$$

where the momenta U_0 are defined by the maps:

$$\begin{aligned} \bar{\pi}_-^{-1}(q, \phi, \bar{p}, \Phi) &= (\pi_-^{-1}(q), \phi, 2A(\pi_-^{-1}(q))^T(\bar{p}, 0), \Phi) \\ \bar{\pi}_+^{-1}(q, \phi, \bar{p}, \Phi) &= (\pi_+^{-1}(q), \phi, 2A(\pi_+^{-1}(q))^T(\bar{p}, 0), \Phi) \end{aligned} \quad (57)$$

with

$$\bar{p} = (p_1, p_2 - 1 + \mu, p_3), \quad (58)$$

i.e.,

$$\begin{aligned} U_{1,0} &= 2(u_{1,0}p_{1,0} + u_{2,0}(p_{2,0} - 1 + \mu) + u_{3,0}p_{3,0}) \\ U_{2,0} &= 2(u_{1,0}(p_{2,0} - 1 + \mu) - u_{2,0}p_{1,0} + u_{4,0}p_{3,0}) \\ U_{3,0} &= 2(u_{1,0}p_{3,0} - u_{3,0}p_{1,0} - u_{4,0}(p_{2,0} - 1 + \mu)) \\ U_{4,0} &= 2(u_{2,0}p_{3,0} - u_{3,0}(p_{2,0} - 1 + \mu) + u_{4,0}p_{1,0}) \end{aligned} \quad (59)$$

- (iii) **Numerical integration.** The numerical integration of the Hamilton equations of the regularized Hamiltonian \mathcal{K} provides a sequence $(u_k, \phi_k, U_k, \Phi_k)$ approximating the solution at $s = s_k$. The numerical integration provides also the sequence f_k of the original independent variable f corresponding to the s_k . In fact, from the Hamilton equation:

$$\frac{d\phi}{ds} = \frac{\partial \mathcal{K}}{\partial \Phi} = \|u\|^2,$$

we have $f(s_k) = \phi(s_k)$.

- (iv) **Cartesian solutions by KS back-transformation.** Retrieve the solutions of the Hamilton equations of the original Hamiltonian \mathcal{H} via projection:

$$\begin{cases} x_k = u_{1,k}^2 - u_{2,k}^2 - u_{3,k}^2 + u_{4,k}^2 + 1 - \mu \\ y_k = 2u_{1,k}u_{2,k} - 2u_{3,k}u_{4,k} \\ z_k = 2u_{3,k}u_{1,k} + 2u_{4,k}u_{2,k} \\ p_{1,k} = \frac{1}{2\|u_k\|^2}(u_{1,k}U_{1,k} - u_{2,k}U_{2,k} - u_{3,k}U_{3,k} + u_{4,k}U_{4,k}) \\ p_{2,k} = \frac{1}{2\|u_k\|^2}(u_{2,k}U_{1,k} + u_{1,k}U_{2,k} - u_{4,k}U_{3,k} - u_{3,k}U_{4,k}) + 1 - \mu \\ p_{3,k} = \frac{1}{2\|u_k\|^2}(u_{3,k}U_{1,k} + u_{4,k}U_{2,k} + u_{1,k}U_{3,k} + u_{2,k}U_{4,k}) \end{cases} \quad (60)$$

at the sample points $f_k = f(s_k)$.

4.2. The advantage of the regularization: a numerical test

In order to assess the effectiveness of KS regularization of the ER3BP near the singularity at P_2 for numerical integrations we consider a fictitious simple scenario which is nevertheless representative (for the choice of the initial conditions) of realistic close encounters in the Solar System, such as the non-coplanar close encounters of comets with Jupiter, in the Sun-Jupiter ER3BP (here identified by the values $\mu = 9.536433730801362 \cdot 10^{-4}$, $\varepsilon = 0.0489$). Precisely we consider the case, critical for the numerical integrations, of fast close encounters, where here we mean ‘fast’ both in the sense of Section 3 (see the caption of Fig. 1) and that the close encounter does not produce a temporary capture through the Lagrangian points L_1, L_2 . We emphasize that fast close encounters are observed for celestial bodies in the Solar System (see for example [24,25] where the dynamics of comet 67P Churyumov-Gerasimenko, target of the recent Rosetta mission, is discussed in detail), and are used in Astrodynamics to accelerate spacecrafts.

In this Section we consider a model example numerically integrated using a quadruple precision floating-point format with an explicit fixed step numerical integrator of the Runge–Kutta family (Luther’s method [46], RK6 for brevity) to analyze possible gains in the use of the KS regularization. The choice of using explicitly a fixed step integrator is motivated by the need to avoid any interference of a variable step strategy with the regularization, which automatically performs the reduction of the step size by adopting a fictitious independent variable. We also remark that, even if the RK6 integrator is not symplectic, it does not produce a relevant energy loss since fast close encounters occur in small time intervals.

Therefore, we choose orbits with initial conditions characterized by a high initial energy $\mathcal{E} > \mathcal{E}_4 := J(x_{L_4}, y_{L_4}, z_{L_4}, x'_{L_4}, y'_{L_4}, z'_{L_4}, f_0)$, where J is the f -dependent Jacobi “integral”⁵:

$$J(x, y, z, x', y', z', f) = \frac{1}{2} ((x')^2 + (y')^2 + (z')^2) - \frac{1}{1 + \varepsilon \cos f} \left(\frac{1 - \mu}{d_1} + \frac{\mu}{d_2} + \frac{1}{2} (x^2 + y^2 - z^2 \varepsilon \cos f) \right), \quad (61)$$

having, in the vicinity of the secondary body, an important deflection of the trajectory with respect to the solutions of the Kepler problem defined by the Sun. Moreover, we consider orbits which are non-planar with Jupiter’s orbit. An efficient way to visualize the outcome of the regularization on fast close encounters is to consider the initial conditions already at their minimum distance from Jupiter, with $\mathcal{E} > \mathcal{E}_4$, with inclination different from 0, then to numerically integrate the orbit by first running a backward integration up to a sufficiently large distance (at least $d_2 = \|P - P_2\| > 1 = \|P_2 - P_1\|$), and then to switch to a forward integration lasting exactly twice the number of integration steps of the previous operation, so that the upshot produces almost equal-length branches before and after the encounter (blue and red lines in top panels of Fig. 1). In such a way, we appreciate the whole dynamics with the deviation caused by the planet. More details on the choice of the initial conditions are given in the caption of Fig. 1; the physical parameters are drawn from the NASA Planetary Fact Sheet.⁶ The details of implementation of the numerical integration, including also the formulas for the computation of the initial condition in (u, ϕ, U, Φ) variables for any given Cartesian initial condition (x, y, z, p_1, p_2, p_3) , are as described in Section 4.1.

⁵ We recall that J is not a first integral for the eccentricities $\varepsilon > 0$; therefore, the choice $\mathcal{E} > \mathcal{E}_4$ provides only a trial initial condition for having a fast close encounter.

⁶ <https://nssdc.gsfc.nasa.gov/planetary/factsheet/>

In Figs. 1 and 2 we illustrate the particle’s orbit: we set initial values so that the planetary flyby is of hyperbolic gravity-assist type and the heliocentric paths before and after the encounter are almost Keplerian ellipses.

In Table 1 we compare the numerical integration of the close encounter represented in Figs. 1 and 2 using both the Cartesian and the KS regularized equations of motion on a smaller true anomaly range, for different values of the integration steps. Precisely, using as initial condition the point of closest approach, we integrate the equations of motion backward up to $f_- \approx -0.5$, and then forward up to $f_+ \approx 0.5$, since $f_+ - f_- \approx 1$ represents approximately the interval of the true anomaly in which the close encounter takes place. We compare both the conservation of the extended Hamiltonians $\hat{H} = H + \Phi$, $\hat{\mathcal{K}}$ and the value of $\|r\|$, $r = (x, y, z)$, at the end of the two numerical integrations. Since the numerical integration of the Cartesian equations of motion is carried out with a fixed step Δf , while the numerical integration of the regularized equations of motion is carried out with a fixed step Δs , in order to compare the outputs of the two numerical integrations at the same values of f we add a further integration step to the Cartesian numerical integration to reach the final value of f obtained with the KS numerical integration. We note the sharp advantage of the KS algorithm in terms of computational efficiency, providing a sharp reduction of the number of integration steps needed to maintain a high level of accuracy in the representation of the trajectory around P_2 . Remarkably, it appears that the conservation of the (non-regularized) Hamiltonian is definitely better in the KS integration than in the Cartesian one. Reaching the precision obtained with the KS variables in the Cartesian propagation is way more demanding from a computational viewpoint: by continuing the step size refinement in the first column of the bottom panel of the table, with $\Delta f = 2\pi \cdot 10^{-7}$ we obtain $|\hat{H}(-0.5066821124431412)| = 1.0520763745 \cdot 10^{-24}$ and $|\hat{H}(0.4961307051398083)| = 1.0506642999 \cdot 10^{-24}$, while only with $\Delta f = 2\pi \cdot 10^{-8}$ we improve the performance about the conservation of the Hamiltonian obtained with the KS algorithm for $\Delta s = \pi \cdot 10^{-4}$.

We finally argue that, to maximize the computational efficiency in a long simulation, one should implement as usual a switching tool which works with the \mathcal{H} -equations out of a ball centered at P_2 , say the body’s Hill’s sphere, and the \mathcal{K} -equations once inside.

As conclusive remark, since \mathcal{K} and l are smooth functions in a neighborhood of P_2 , we get that the invariances given by $\mathcal{K}(u, \phi, U, \Phi) = 0$, $l(u, U) = 0$ are numerically satisfied with high precision, and eventually the machine precision is quickly reached after lowering Δs by about a factor of a hundredth (in a convergence profile, the rate of decay reflects the accuracy of the method, i.e., $\mathcal{O}(\Delta s^6)$).

4.3. Detection of multiple close encounters with RFLIs

Regularized fast Lyapunov indicators, introduced in [28,33,34] (see also [35]), are defined for the ER3BP by:

$$\text{RFLI}(\xi_0, w_0; f_0, F) = \max_{f_0 \leq f \leq F} \log_{10} \frac{\|w(s(f))\|}{\|w_0\|}, \quad (62)$$

where:

- $\xi_0 = (r_0, r'_0)$ is the initial position and initial velocity vector given in Cartesian coordinates; f is the true anomaly of the elliptic motion and f_0, F its initial and final values; $s(f)$ denotes the proper time expressed as a function of f ;
- $w(s)$ is the solution of the variational equations of Hamiltonian \mathcal{K} obtained from the variational matrix (6) with initial conditions $w(s(f_0)) = w_0$, computed for an orbit with initial conditions $u(f_0), \phi(f_0), U(f_0), \Phi(f_0)$ provided by a local inversion of the KS transformation (cf. (57), (54), (58) in Section 4.1; by changing the local inversion map, a change in the initial tangent vector should be applied accordingly, see [37]; however, in the experiments below we do not need to apply any local inversion map for the

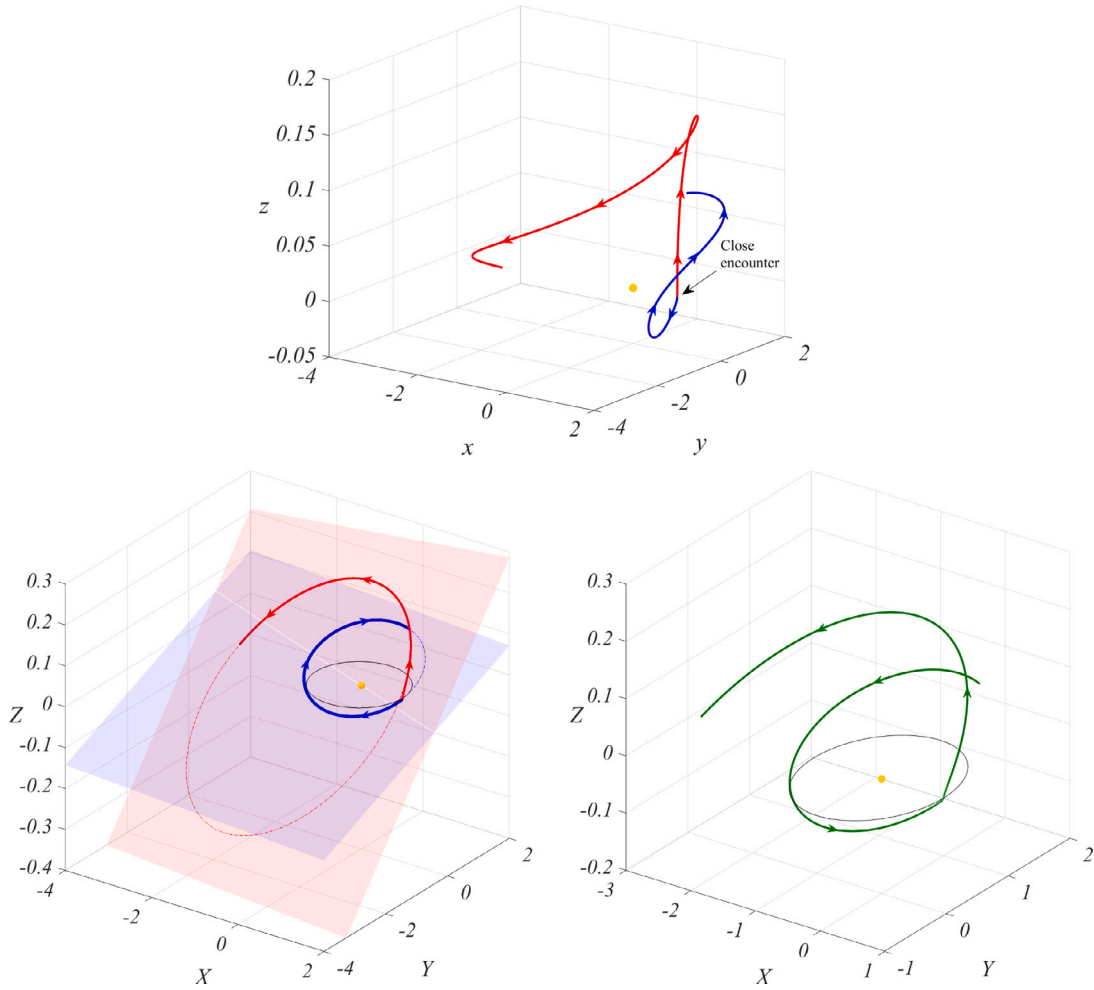


Fig. 1. Physical orbit (reported in convenient aspect ratio for visual clarity) integrated backward in true anomaly up to $f = -2\pi$ and then forward up to $f = 2\pi$ following the arrow heads for $x_0 = 1 - \mu + 1.921451079855507 \cdot 10^{-3}$ (≈ 0.01 AU of altitude), $y_0 = z_0 = f_0 = 0$, $p_{1,0} = 0.2$, $p_{2,0} = 1.8$, $p_{3,0} = 0.6$. The corresponding KS-transformed quadruple precision initial data are:

$$\begin{aligned} u_1 &= 0.0438343595807618585658005372351908591, \\ U_1 &= 0.0175337438323047538346610707549189101, \\ U_2 &= 0.0702185800222737827036567637151165400, \\ U_3 &= 0.0526012314969142580345362603111425415, \\ \Phi &= -1.38220656687993415599045818608844111, \\ u_2 &= u_3 = u_4 = \phi = U_4 = 0. \end{aligned}$$

The yellow dot symbolizes the Sun, whereas the black thin style curve represents Jupiter's elliptic motion. **Top panel:** Cartesian version (backward in blue overlapping the forward in red) traced in the rotating-pulsating frame $Oxyz$. **Left bottom panel:** Cartesian backward (blue) and forward (red) trajectory in the inertial barycentric frame $OXYZ$ (Appendix) with osculating heliocentric ellipses belonging to mutually inclined planes. **Right bottom panel:** KS integration of the inertial trajectory in the forward case. The close encounter is of hyperbolic type (fast): $\Gamma_0 = 1.4282186 \leq \Gamma_s \leq \Gamma_s|_{\min d_2} < (3/2)\Gamma_0$ in $B(\mu^{\frac{1}{3}})$.

choice of the initial tangent vector and it suffices to fix the same vector in \mathbb{R}^8 for all the integrations, see [37] for more details).

According to [25,36,37,47], we also consider the modified indicator mFLI which is suitable to detect the fast close encounters of the ER3BP:

$$\text{mFLI}_\chi(\xi_0, w_0; f_0, F) = \max_{f_0 \leq f \leq F} \int_0^{s(f)} \chi(q(f(s))) \frac{w(s) \cdot \frac{dw}{ds}(s)}{\|w(s)\|^2} ds, \quad (63)$$

where:

- $q(f) = r(f) - (1 - \mu, 0, 0)$ represents the solution of the equations of motion with initial conditions ξ_0 ;
- $f(s)$ is the true anomaly of the elliptic motion expressed as a function of s ;

- $\chi(q)$ is a function depending on a parameter $\lambda > 0$:

$$\chi(q) = \begin{cases} 1 & \text{if } \|q\| \leq \frac{\lambda}{2}, \\ \frac{1}{2} \left[\cos \left(\left(\frac{\|q\|}{\lambda} - \frac{1}{2} \right) \pi \right) + 1 \right] & \text{if } \frac{\lambda}{2} < \|q\| \leq \frac{3}{2} \lambda, \\ 0 & \text{if } \|q\| > \frac{3}{2} \lambda, \end{cases} \quad (64)$$

where $\|q\| = d_2$ is the Cartesian distance $\|P - P_2\|$ and λ is a parameter, that for close encounters is conveniently set as from 1 to 2 Hill's radii r_h of P_2 .

In the following experiments, we aim to detect multiple fast close encounters for small values of $\mu < 1/10$ using the indicators RFLI and mFLI above. We consider the Sun-Earth spatial ER3BP ($\mu = 3.00347 \cdot 10^{-6}$, $\varepsilon = 0.0167$).

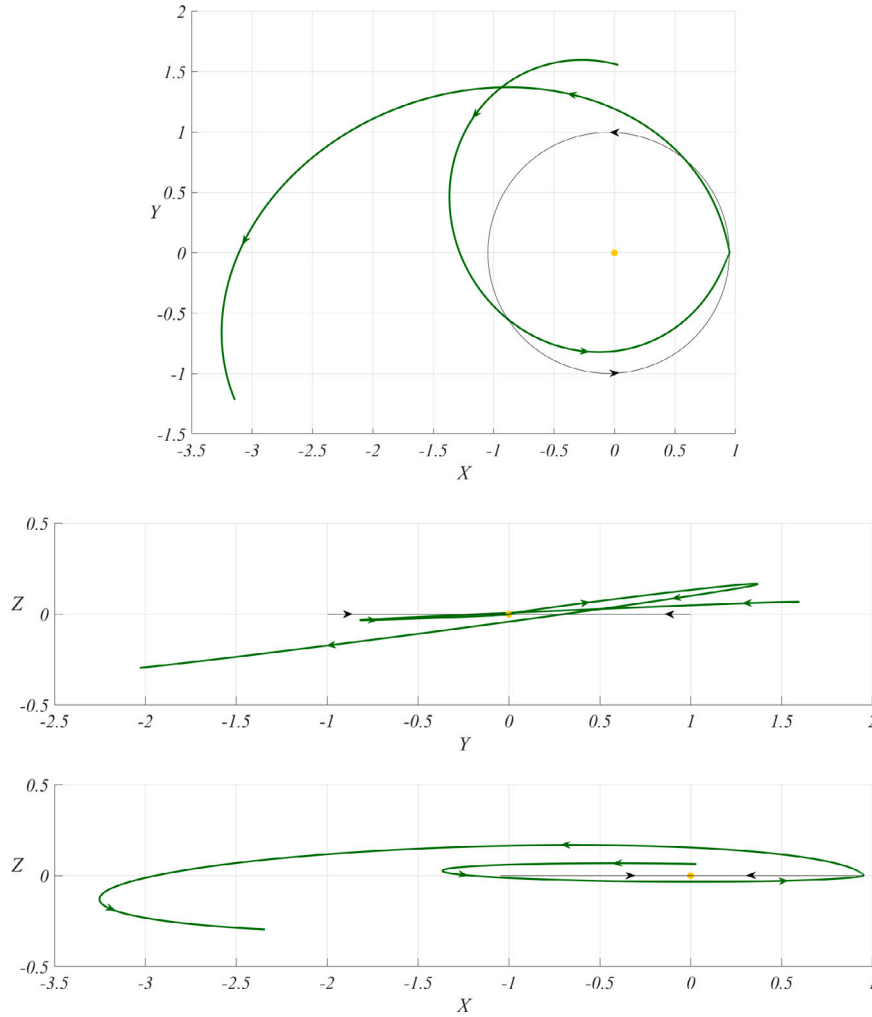


Fig. 2. Projections on the coordinate planes of the right bottom panel of Fig. 1 on equal axis aspect ratio.

We start from a planar reference orbit characterized by a remarkably fast close encounter with the Earth, i.e., with $\Gamma_0 > 0$ sufficiently large entering the Hill's sphere; then we suitably vary initial conditions (x, x') in a neighborhood of those of the reference orbit to explore the nearby phase-space. We take initial conditions corresponding to a 2 : 3 mean-motion resonant orbit in the Keplerian approximation intersecting the Earth's orbit, with pericenter interior to the Earth's trajectory and aligned with the planet's one on the X -axis of the inertial frame. We synchronize times in order to have an exact collision in the future at the first intersection on the Keplerian ellipses by starting with P and P_2 located well apart, say, for convenience, at a relative distance $\|P - P_2\|(f_0) = 1/\sqrt{2} > \|P_2 - P_1\|(0)/2 = (1 - \varepsilon)/2$ expressed in the inertial frame. The resulting orbit is integrated in Fig. 3, complemented by Γ_s during the Hill's sphere crossing.

At this stage, we compute the indicator (63) on a grid of initial conditions (x, x') equally spaced in the two coordinates, while keeping fixed y, z, y', z' and setting $\Phi = -\mathcal{H}(x, y, z, p_1, p_2, p_3, f_0)$ to perform the regularization. We slightly move away from the reference orbit until the mFLI portrays fast close encounter structures in the phase-space and we therein increase the resolution. Additionally, for a better visualization and to include multiple close encounter orbits, we extend the integration interval from f_0 up to $F = f_c + 15\pi + 2$, with f_0, f_c given in the caption of Fig. 3. The outcome reproducing fast close encounter loci is reported in the top panel of Fig. 4.

The spatial continuation of these loci can be inspected by integrating orbits with nonzero initial z' (or z) starting from the planar structures. In the bottom panel of Fig. 4 we compute such continuations in the (x, z') section for positive and negative z' upon setting, respectively, $x' = x'_{\max}$ and $x' = x'_{\min}$ for all the grid points, where $x' \in [x'_{\min}, x'_{\max}]$ in the planar chart.

The lobes depicted in Fig. 4 correspond to single or multiple close encounter orbits, as well as to deeper or less deep encounters. We explore the nature of these lobes by considering the sample orbits (indicated in the same figure) ℓ_M, ℓ_L, ℓ_U when $z' = 0$, ℓ_M^+, ℓ_U^+ when $z' > 0$ and ℓ_M^-, ℓ_L^- when $z' < 0$. We plot in Fig. 5 $\Gamma_s, \text{RFLI}(s), \text{mFLI}(s)$ for $s \in [0, s(F)]$ and $d_2(s)$ in a neighborhood containing the Hill's sphere for each selected orbit.

In the top left panel, we can distinguish between orbits facing either 1, 2 or 3 close encounters with the Earth by looking at their variation of Γ_s in the Hill's sphere (almost null, see Fig. 3), which fulfills the properties of Section 3, so we verify the hyperbolicity of each encounter. The occurrences, position and length of each colored line provide information on the number, moment and duration in proper time of the corresponding encounters along every orbit, where by 'duration' we mean the time spent in the Hill's sphere. For an easier identification, orbits are listed in the legend according to the same order as the heights of the colored lines appear in the plot, grouped by lobe name (label 'U' as 'upper', label 'M' as 'middle', label 'L' as 'lower').

Table 1

Comparison between Cartesian and KS integration for four consecutively increased step sizes in a small neighborhood of $f = s = 0$ (close approach). The propagations are performed backward in time up to $f(-3.7\pi) = -0.506682112443141208003735413674982089$, then forward up to $f(3.5\pi) = 0.496130705139808336532715403656106249$, according to choices of s such that the true anomaly interval is almost symmetric with respect to the origin and sample nodes are multiple integers of every Δs considered. For each case the step size is eventually adapted in order to evaluate the singular and regularized solution at same corresponding times (see text). The asterisk in the last Cartesian experiment indicates failure of the adopted numerical method (explicit RK6) to compute the orbit accurately. **Top panel:** norm of the solutions (rounded to 16 significant digits) and total number of integration steps. **Bottom panel:** degree of conservation of the singular extended Hamiltonians (rounded to 11 significant digits), where $\hat{H}(0) = \hat{\mathcal{H}}(0) = 0$.

Δf (Cart.)	$\ r(-0.5066821124431412)\ $	$\ r(0.4961307051398083)\ $	# steps
$2\pi \cdot 10^{-6}$	0.8553075048550535	0.9760051057296899	240 244
$2\pi \cdot 10^{-5}$	0.8553075048542582	0.9760051057288172	24 026
$2\pi \cdot 10^{-4}$	0.8553060796173549	0.9760054080001320	2404
$2\pi \cdot 10^{-3}$ (*)	0.8248588821498852	0.9897100124542644	241
Δs (KS reg.)	$\ r(f(-3.7\pi))\ $	$\ r(f(3.5\pi))\ $	# steps
$\pi \cdot 10^{-4}$	0.8553075048550521	0.9760051057296942	109 000
$\pi \cdot 10^{-3}$	0.8553075048550521	0.9760051057296942	10 900
$\pi \cdot 10^{-2}$	0.8553075048550522	0.9760051057296968	1090
$\pi \cdot 10^{-1}$	0.8553075050607468	0.9760051591505222	109

Δf (Cart.)	$ \hat{H}(-0.5066821124431412) $	$ \hat{H}(0.4961307051398083) $
$2\pi \cdot 10^{-6}$	$1.0417562295 \cdot 10^{-18}$	$1.0277827090 \cdot 10^{-18}$
$2\pi \cdot 10^{-5}$	$9.3757489321 \cdot 10^{-13}$	$7.9843639352 \cdot 10^{-13}$
$2\pi \cdot 10^{-4}$	$1.1893484533 \cdot 10^{-7}$	$8.5748939646 \cdot 10^{-7}$
$2\pi \cdot 10^{-3}$ (*)	$8.0281428133 \cdot 10^{-2}$	0.10590853333
Δs (KS reg.)	$ \hat{\mathcal{H}}(-3.7\pi) $	$ \hat{\mathcal{H}}(3.5\pi) $
$\pi \cdot 10^{-4}$	$1.3746151644 \cdot 10^{-27}$	$1.3290033656 \cdot 10^{-28}$
$\pi \cdot 10^{-3}$	$1.3738069068 \cdot 10^{-21}$	$1.3119148531 \cdot 10^{-22}$
$\pi \cdot 10^{-2}$	$1.3654070424 \cdot 10^{-15}$	$1.1227698042 \cdot 10^{-16}$
$\pi \cdot 10^{-1}$	$1.2545211218 \cdot 10^{-9}$	$3.0569361253 \cdot 10^{-10}$

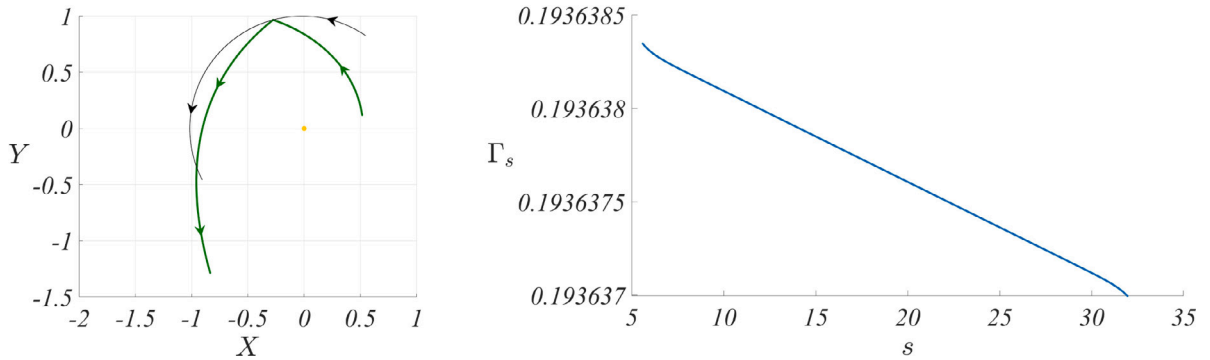


Fig. 3. Reference orbit for mFLI/RFLI computations in the Sun-Earth system. **Left panel:** Cartesian orbit in the inertial barycentric frame $OXYZ$ (green) approaching the Earth (black thin) at $f_c \approx 106^\circ$ from $f_0 = 0.9862623425908257$. The initial orbital elements of the test particle are: $a_P(f_0) = 1.3103706971044482$ (semi-major axis), $e_P(f_0) = 0.6$ (eccentricity), $f_P(f_0) = 0.22823102675215523$ (true anomaly), $i_P(f_0) = \omega_P(f_0) = \Omega_P(f_0) = 0$ (inclination, argument of pericenter, longitude of the ascending node). The yellow dot represents the Sun. **Right panel:** trend of $\Gamma_s > 0$ throughout the fast close encounter (note, indeed, that $\Gamma_s \approx \Gamma_0 = 0.1936383474044529 \in [\Gamma_0/2, 3\Gamma_0/2]$).

In the bottom left panel, we observe the strong divergence of orbits with close initial conditions for all the orbits pinpointed by a growing RFLI.

In the bottom right panel, we can appreciate the strength of the encounters by looking at the mFLI jumps of the orbits. Qualitatively, we can better determine the depth of the approaches by comparing their

minimum distance d_2 in the top right panel. Examining the two panels altogether, we observe that:

- of the three close encounters of orbits on the planar upper lobe (ℓ_U , magenta curve), the first taking place is weak (justified by a large minimum distance d_2 and a small jump in the mFLI),

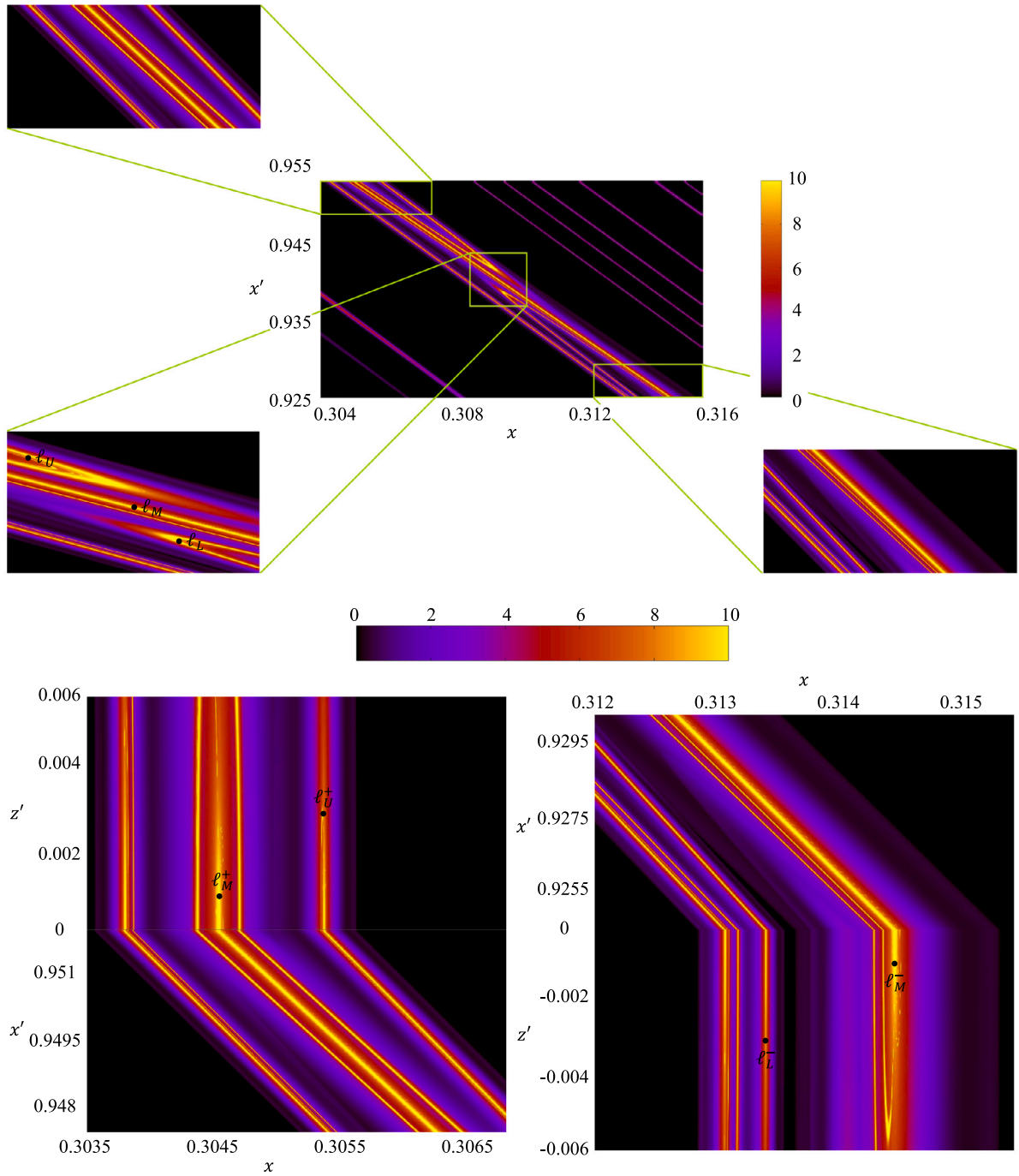


Fig. 4. $mFLI_\chi$ charts of the Sun-Earth ER3BP over 1000×1000 regularly spaced initial conditions close to those of Fig. 3. Here $\lambda = r_H$ in χ and $w_0 \in \mathbb{S}^7$. **Top panel:** planar section with three magnifications of the close encounter lobes emerging diagonally in the figure. In the central magnification we discern three main lobes (middle, lower, upper), on which sample orbits ℓ_M , ℓ_L , ℓ_U are taken, respectively. **Bottom panel:** spatial sections merged to corresponding above planar magnifications of the main lobes. The effect is a continuation of the close encounter structures along the z' -axis. Sample orbits ℓ_M^+ , ℓ_L^+ , ℓ_U^+ are taken on the positive z' extensions of the main lobes (left), while sample orbits ℓ_M^- , ℓ_L^- , ℓ_U^- are taken on the negative z' extensions of the main lobes (right).

the second and the third are definitely stronger by similar considerations, though they are not the strongest if compared to other encounters in the pictures, thus, we term them medium; analogously, of the two close encounters of orbits on the spatial upper lobe (ℓ_U^+ , blue curve), the first taking place can be classified as medium and the second as weak;

- the single close encounter of orbits on the middle lobe, both planar and spatial (ℓ_M , ℓ_M^+ , ℓ_M^- ; black, dark yellow and green curves, respectively), turns out to be very deep, more than those of the upper lobe orbits;

- the orbits on the planar lower lobe (ℓ_L , cyan curve) present a double close encounter of which the first is the weakest of the figure, the second is, by contrast, the strongest (respectively, minimum and maximum values of the mFLI jumps); the orbits on the spatial lower lobe (ℓ_L^- , red curve) experience one medium-deep close encounter, in the sense that the mFLI jump and the minimum of d_2 attain intermediate values between those attributed, so far, to medium and strong approaches.

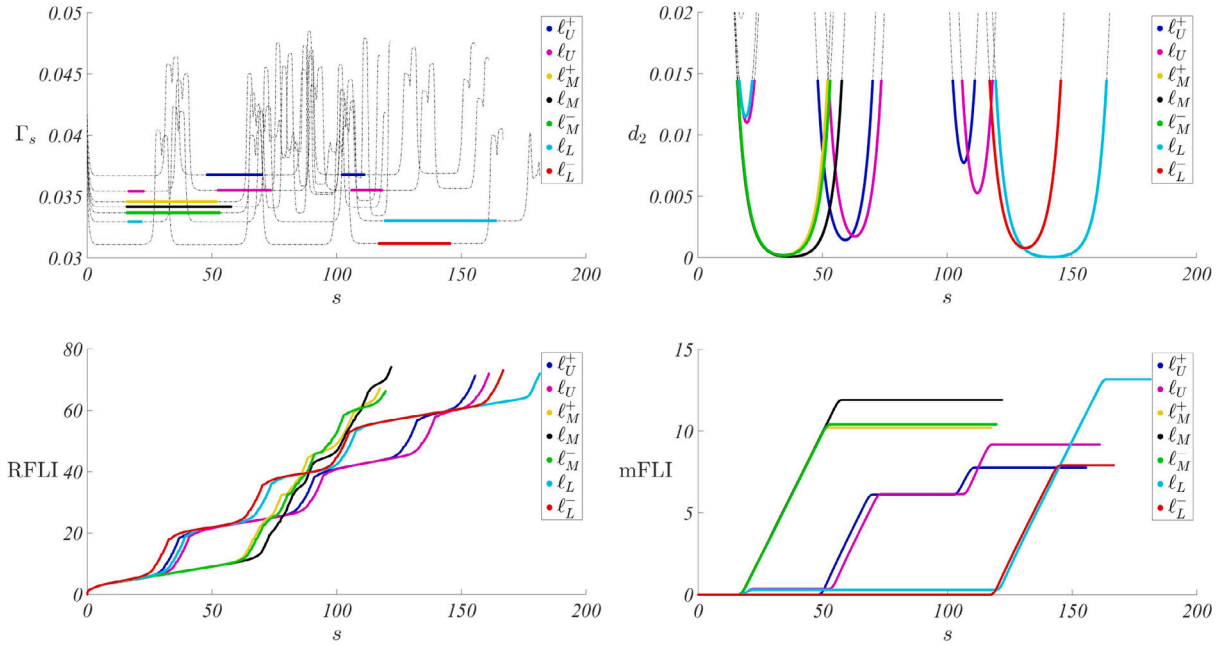


Fig. 5. Γ_s , d_2 , RFLI and mFLI as functions of s for the sample orbits of Fig. 4. **Top left panel:** Γ_s along the whole propagation (dashed) and in $B(\mu^{1/3})$ (solid colored). **Top right panel:** $d_2(s)$ in $B(\mu^{1/3})$ (solid colored) and graph continuations outside $B(\mu^{1/3})$ (dashed). **Bottom left panel:** RFLI(s). **Bottom right panel:** mFLI(s).

According to this analysis, the development of the dynamics in the third spatial dimension appears to reduce the chance for fast close encounters, which seems intuitive given the extra degree of freedom coming into play. Nonetheless, it is worth mentioning that an intrinsic limitation is due to the finite resolution of the portraits in Fig. 4: more refined grids reveal further distinct branches inside the visible lobes with possible different dynamical features in terms of close encounter detection.

The last result that we report is Fig. 6. On the same grid (x, x') of the central zoom-in of top panel of Fig. 4, we compute the Tisserand parameter

$$\mathcal{T} = \frac{1}{a_p} + 2 \cos i_p \sqrt{a_p(1 - e_p^2)} \quad (65)$$

at final value $f = F$, which is subject to a more significant variation when close approaches occur. Comparing the two panels of the figure, we can notice that only fewer and less detailed structures are replicated, like the three main lobes identified above, corresponding to the deepest encounters. This further supports the effectiveness of the indicator (63). The brighter lines in the bottom panel indicate the exact match between the upper, middle and lower lobes of the two overlapped plots.

5. Proofs of Section 3

5.1. Proof of inequalities (44), (45), (46), (47)

Inequalities (45) and (46) follow immediately from the fact that the vector $b(u)$ is cubic in the u_i . Indeed:

$$\|b\|^2 = |b \cdot b| = 4 \|u\|^2 |Au \cdot A^2 Au| \leq 4 \|u\|^6$$

thanks to $\|A\|^2 = 1$ (operator norm induced by the Euclidean vector norm), (13) and Cauchy-Schwarz inequality, so it suffices that $c_2 \geq 2$. Consequently, $|\partial b_i / \partial u_j| \leq c_* \|u\|^2$, $c_* > 0$, thus (46) holds.

To prove inequalities (44) and (47) we first replace in \mathcal{R}_6 the only non-polynomial term with its Taylor expansion of order 1 in the π_1, π_2, π_3 with remainder Δ_4 (of order 2 in the π_j , of order 4 in the u_i):

$$\frac{1}{\|\pi + (1, 0, 0)\|} = \frac{1}{\sqrt{(\pi_1 + 1)^2 + \pi_2^2 + \pi_3^2}} = 1 - \pi_1 + \Delta_4, \quad (66)$$

and we obtain:

$$\mathcal{R}_6 = -\frac{\|u\|^2}{1 + \varepsilon \cos \phi} \left[(1 - \mu) \Delta_4 + \frac{1}{2} (\pi_1^2(u) + \pi_2^2(u) - \pi_3^2(u) \varepsilon \cos \phi) \right]. \quad (67)$$

Since for $\mu \leq \mu_0 < 1/10$ we have $d_2 < (1/10)^{1/3} < 1/2$, $d_1 > 1/2$ in $B(\mu^{1/3})$ as well as:

$$1 - d_1(\pi_1 - 1) = 1 + d_1 - d_1\pi_1 \geq 1 + d_1(1 - d_2) > 1,$$

we obtain:

$$|\Delta_4| = \left| \frac{1}{d_1} + \pi_1 - 1 \right| = \left| \frac{1 + d_1(\pi_1 - 1)}{d_1} \right| = \left| \frac{1 - d_1^2(\pi_1 - 1)^2}{d_1(1 + d_1 - d_1\pi_1)} \right| < 2 |1 - d_1^2(\pi_1 - 1)^2|.$$

Since $1 - d_1^2(\pi_1 - 1)^2$ is a polynomial in π_1, π_2, π_3 with terms of order 2, 3, 4, there exists a constant γ_1 such that:

$$|\Delta_4| \leq \gamma_1 \|u\|^4. \quad (68)$$

Inequality (44) follows easily.

We proceed by estimating the derivatives of Δ_4 :

$$\frac{\partial \Delta_4}{\partial u_j} = \sum_{h=1}^3 \frac{\partial \Delta_4}{\partial \pi_h} \frac{\partial \pi_h}{\partial u_j}.$$

Since the π_h are quadratic function of the u_j , with $|\pi_h| \leq \|u\|^2$, and since $1 - d_1^6$ is a polynomial containing terms of least order in the π_i equal to 1, there exists a positive constant γ_* such that:

$$|1 - d_1^6| \leq \gamma_* \|u\|^2 \quad (69)$$

and a positive constant γ_2 such that:

$$\left| \frac{\partial \Delta_4}{\partial \pi_2} \frac{\partial \pi_2}{\partial u_j} \right| = \left| \frac{\pi_2}{d_1^3} \frac{\partial \pi_2}{\partial u_j} \right| < 8 |\pi_2| \left| \frac{\partial \pi_2}{\partial u_j} \right| \leq \gamma_2 \|u\|^3,$$

$$\left| \frac{\partial \Delta_4}{\partial \pi_3} \frac{\partial \pi_3}{\partial u_j} \right| = \left| \frac{\pi_3}{d_1^3} \frac{\partial \pi_3}{\partial u_j} \right| < 8 |\pi_3| \left| \frac{\partial \pi_3}{\partial u_j} \right| \leq \gamma_2 \|u\|^3,$$

$$\left| \frac{\partial \Delta_4}{\partial \pi_1} \frac{\partial \pi_1}{\partial u_j} \right| = \left| \frac{1 + \pi_1 - d_1^3}{d_1^3} \frac{\partial \pi_1}{\partial u_j} \right| < 8(|\pi_1| + |1 - d_1^3|) \left| \frac{\partial \pi_1}{\partial u_j} \right|$$

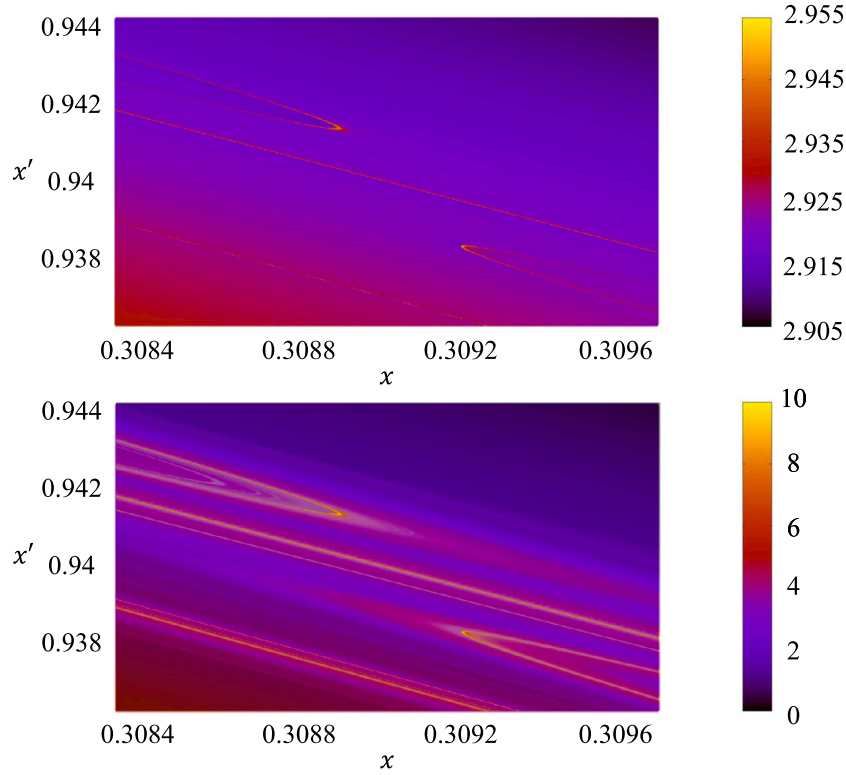


Fig. 6. $\mathcal{T}(F)$ from (65) over the mFLI central magnification in the planar case. **Top panel:** $\mathcal{T}(F)$ chart. **Bottom panel:** Faded representation of the top panel ($\mathcal{T}(F)$) overlapped to the corresponding mFLI_x chart from Fig. 4.

$$\begin{aligned}
 &= 8 \left(|\pi_1| + \frac{|1 - d_1^6|}{1 + d_1^3} \right) \left| \frac{\partial \pi_1}{\partial u_j} \right| \\
 &< 8 \left(|\pi_1| + |1 - d_1^6| \right) \left| \frac{\partial \pi_1}{\partial u_j} \right| \leq \gamma_2 \|u\|^3.
 \end{aligned}$$

Inequality (47) follows straightforwardly.

5.2. Proof of inequality (48)

$$\begin{aligned}
 \text{In:} \\
 \frac{d\Gamma_s}{ds} &= \frac{\partial \mathcal{K}}{\partial \phi} + \frac{(3 - 4\mu + \mu^2)\epsilon \sin \phi}{2(1 + \epsilon \cos \phi)^2} \frac{\partial \mathcal{K}}{\partial \Phi} \\
 &= -\frac{\epsilon \sin \phi}{(1 + \epsilon \cos \phi)^2} \left((1 - \mu) \|u\|^2 \left(\frac{1}{\|\pi(u) + (1, 0, 0)\|} + \pi_1(u) \right) \right. \\
 &\quad + \mu + \frac{1}{2} \|u\|^2 (\pi_1^2(u) + \pi_2^2(u) - \pi_3^2(u) \epsilon \cos \phi) + \frac{(1 - \mu)^2}{2} \|u\|^2 \\
 &\quad \left. + \frac{1}{2} (1 + \epsilon \cos \phi) \|u\|^2 \pi_3^2(u) - \frac{3 - 4\mu + \mu^2}{2} \|u\|^2 \right) \quad (70)
 \end{aligned}$$

we first replace the only non-polynomial term with the representation (66), and then we simplify the expression obtaining:

$$\frac{d\Gamma_s}{ds} = -\frac{\epsilon \sin \phi}{(1 + \epsilon \cos \phi)^2} \left(\mu + \|u\|^2 (1 - \mu) \Delta_4 + \frac{1}{2} \|u\|^2 \|\pi\|^2 \right). \quad (71)$$

Using (68), $\|\pi\|^2 = \|u\|^4$, and $\|u\| < \mu^{\frac{1}{6}}$ in the Hill's sphere (as well as $1 - \mu < 1$), we easily obtain (48).

5.3. Proof of inequality (52)

First, we represent $d^2\rho/ds^2 = 2u \cdot d^2u/ds^2 + 2\|du/ds\|^2$ by replacing d^2u/ds^2 using the Hamilton equations of \mathcal{K} given in the form (39):

$$\frac{d^2\rho}{ds^2} = \Gamma_s \|u\|^2 + 2 \left\| \frac{du}{ds} \right\|^2 + \frac{1}{8} \sum_i (U_i - b_i) \sum_j u_j \left(\frac{\partial b_i}{\partial u_j} - \frac{\partial b_j}{\partial u_i} \right) - \frac{1}{2} \sum_i u_i \frac{\partial \mathcal{R}_6}{\partial u_i},$$

and then we replace $2\|du/ds\|^2 = (1/8)\|U - b\|^2$ using $\mathcal{K}(u(s), \phi(s), U(s), \Phi(s)) = 0$:

$$\begin{aligned}
 \frac{d^2\rho}{ds^2} &= 2\Gamma_s \|u\|^2 + \frac{\mu}{1 + \epsilon \cos \phi} \\
 &\quad + \frac{1}{8} \sum_i (U_i - b_i) \sum_j u_j \left(\frac{\partial b_i}{\partial u_j} - \frac{\partial b_j}{\partial u_i} \right) - \frac{1}{2} \sum_i u_i \frac{\partial \mathcal{R}_6}{\partial u_i} - \mathcal{R}_6. \quad (72)
 \end{aligned}$$

Using (44), (47) and (46), (50), the terms in the second line of (72) are bounded by:

$$\begin{aligned}
 \left| \frac{1}{2} \sum_i u_i \frac{\partial \mathcal{R}_6}{\partial u_i} + \mathcal{R}_6 \right| &\leq \frac{1}{2} \left| \sum_i u_i \frac{\partial \mathcal{R}_6}{\partial u_i} \right| + |\mathcal{R}_6| \leq \left(c_1 + \frac{1}{2} c_4 \right) \frac{1}{1 - \epsilon} \|u\|^6, \\
 \left| \sum_i (U_i - b_i) \sum_j u_j \left(\frac{\partial b_i}{\partial u_j} - \frac{\partial b_j}{\partial u_i} \right) \right| &\leq \|U - b\| \sum_i \left| \sum_j u_j \left(\frac{\partial b_i}{\partial u_j} - \frac{\partial b_j}{\partial u_i} \right) \right| \leq \\
 &\leq c_3 \|U - b\| \|u\|^3 \leq c_3 c_6 \|u\|^3 \sqrt{\Gamma_0 \|u\|^2 + \frac{\mu}{1 - \epsilon}}.
 \end{aligned}$$

Therefore, using $\Gamma_s \geq \Gamma_0/2$ and (41), there exists a constant γ_3 such that:

$$\begin{aligned}
 \frac{d^2\rho}{ds^2} &\geq \Gamma_0 \|u\|^2 + \frac{\mu}{1 + \epsilon} - \frac{c_3 c_6}{8} \|u\|^3 \sqrt{\Gamma_0 \|u\|^2 + \frac{\mu}{1 - \epsilon}} - \frac{2c_1 + c_4}{2(1 - \epsilon)} \|u\|^6 \\
 &\geq \Gamma_0 \|u\|^2 + \frac{\mu}{1 + \epsilon} - \gamma_3 \|u\|^3 \max \left\{ \|u\| \sqrt{\Gamma_0}, \frac{\sqrt{\mu}}{\sqrt{1 - \epsilon}}, \frac{\sqrt{\mu}}{1 - \epsilon} \right\} \\
 &= \Gamma_0 \|u\|^2 + \frac{\mu}{1 + \epsilon} - \gamma_3 \|u\|^3 \max \left\{ \|u\| \sqrt{\Gamma_0}, \frac{\sqrt{\mu}}{1 - \epsilon} \right\}. \quad (73)
 \end{aligned}$$

Let us now consider the two cases:

- In the case: $\|u\| \sqrt{\Gamma_0} \leq \sqrt{\mu}/(1 - \epsilon)$, inequality (73) becomes:

$$\begin{aligned}
 \frac{d^2\rho}{ds^2} &\geq \Gamma_0 \|u\|^2 + \frac{\mu}{1 + \epsilon} - \gamma_3 \|u\|^3 \frac{\sqrt{\mu}}{1 - \epsilon} \geq \Gamma_0 \|u\|^2 + \frac{\mu}{1 + \epsilon} - \gamma_3 \|u\|^2 \frac{\mu}{(1 - \epsilon)^2 \sqrt{\Gamma_0}} \\
 &\geq \frac{\Gamma_0}{2} \|u\|^2 + \frac{\mu}{1 + \epsilon},
 \end{aligned}$$

where the last inequality is true if we assume:

$$\mu \leq (1 - \varepsilon)^2 \frac{\Gamma_0^{\frac{3}{2}}}{2\gamma_3}. \quad (74)$$

- In the case $\|u\| \sqrt{\Gamma_0} \geq \sqrt{\mu}/(1 - \varepsilon)$, inequality (73) becomes:

$$\begin{aligned} \frac{d^2 \rho}{ds^2} &\geq \Gamma_0 \|u\|^2 + \frac{\mu}{1 + \varepsilon} - \gamma_3 \|u\|^4 \sqrt{\Gamma_0} \\ &\geq \frac{\Gamma_0}{2} \|u\|^2 + \frac{\mu}{1 + \varepsilon}, \end{aligned}$$

where the last inequality is true for all u satisfying:

$$\|u\|^2 \leq \frac{\sqrt{\Gamma_0}}{2\gamma_3},$$

which is satisfied for all $u \in B(\mu^{\frac{1}{6}})$ if $\mu^{\frac{1}{3}} \leq \sqrt{\Gamma_0}/(2\gamma_3)$, or equivalently:

$$\mu \leq \frac{1}{8\gamma_3^3} \Gamma_0^{\frac{3}{2}}. \quad (75)$$

Therefore, we have proved inequality (52) if μ satisfies (74) and (75), which are both satisfied by inequality (51) for any c_7 such that:

$$c_7 \leq \min \left\{ \frac{1}{8\gamma_3^3}, \frac{1}{2\gamma_3} \right\}.$$

5.4. Proof of item (v)

We first restrict the choice of c in the interval $0 < c \leq c_7$, so that (53) is stronger than (51), i.e., the right-hand side of the former is smaller or equal than the one of the latter. As long as Δs satisfies (49) and μ satisfies (53), $\rho(s)$ satisfies (52) and consequently we have:

$$\begin{aligned} \rho(s) - \rho(s_1) &= \frac{d\rho}{ds}(s_1)(s - s_1) + \int_{s_1}^s \left(\int_{s_1}^{\tau} \frac{d^2 \rho}{d\sigma^2}(\sigma) d\sigma \right) d\tau \\ &\geq \frac{d\rho}{ds}(s_1)(s - s_1) + \int_{s_1}^s \left(\int_{s_1}^{\tau} \left(\frac{\Gamma_0}{2} \rho(\sigma) + \frac{\mu}{1 + \varepsilon} \right) d\sigma \right) d\tau. \end{aligned} \quad (76)$$

Since μ satisfies (51) and $\|u(s_1)\| = \mu^{\frac{1}{6}}$, combining Cauchy-Schwarz inequality, Hamilton equations and (50) we have:

$$\begin{aligned} \left| \frac{d\rho}{ds}(s_1) \right| &\leq 2 \|u(s_1)\| \left\| \frac{du}{ds}(s_1) \right\| = \frac{1}{2} \mu^{\frac{1}{6}} \|U(s_1) - b(u(s_1))\| \\ &\leq \frac{c_6}{2} \mu^{\frac{1}{6}} \sqrt{\Gamma_0 \mu^{\frac{1}{3}} + \frac{\mu}{1 - \varepsilon}} \leq c_8 \mu^{\frac{1}{3}} \sqrt{\Gamma_0}, \end{aligned}$$

with c_8 depending only on c_6, c_7 . Therefore, from (76) we obtain:

$$\rho(s) - \rho(s_1) > -c_8 \mu^{\frac{1}{3}} \sqrt{\Gamma_0}(s - s_1) + \frac{\mu}{2(1 + \varepsilon)}(s - s_1)^2. \quad (77)$$

Let us now consider from (77) the inequality:

$$-c_8 \mu^{\frac{1}{3}} \sqrt{\Gamma_0} \omega + \frac{\mu}{2(1 + \varepsilon)} \omega^2 > 0, \quad (78)$$

which is satisfied in particular by all $\omega > \omega_1 > 0$, with:

$$\omega_1 := 2(1 + \varepsilon)c_8 \frac{\sqrt{\Gamma_0}}{\mu^{\frac{2}{3}}}.$$

Since:

$$\omega_1 < 4c_8 \frac{\sqrt{\Gamma_0}}{\mu^{\frac{2}{3}}} =: \omega_2,$$

inequality (78) is satisfied in particular by all $\omega \geq \omega_2$. If μ satisfies the further inequality:

$$\frac{\varepsilon \mu^{\frac{1}{3}}}{(1 - \varepsilon)^2} \leq \frac{\sqrt{\Gamma_0}}{8c_5 c_8}, \quad (79)$$

then the choice for $\Delta s = \omega_2$ satisfies inequality (49). Now we can state that $s_2 \in [s_1, s_1 + \omega_2]$. In fact, if $s_1 + \omega_2 \leq s_2$, then inequality (77) is valid also for $s = s_1 + \omega_2$:

$$\rho(s_1 + \omega_2) > \rho(s_1) = \mu^{\frac{1}{6}},$$

which contradicts the hypothesis $u(s_1 + \omega_2) \in B(\mu^{\frac{1}{6}})$. Therefore, the motion exits from the Hill's sphere at a proper time $s \in (s_1, s_1 + \omega_2)$. Finally we notice that (79) is satisfied if:

$$\mu \leq c_9(1 - \varepsilon)^6 \Gamma_0^{\frac{3}{2}}, \quad (80)$$

with suitable constant c_9 , and therefore both inequalities (80) and (51) are satisfied by the μ satisfying (53), provided that $c < \min\{c_7, c_9\}$.

6. Conclusions

We constructed a local geometric Kustaanheimo-Stiefel regularization of the spatial ER3BP using a (symplectic) iso-energetic reduction of the phase-space. Out of this construction, we obtained an algorithm to efficiently apply the regularization to close encounter solutions. Subsequently, using the developed KS formalism, we extended the characterization of fast close encounters with the secondary body originally conceived in the CR3BP to the ER3BP, by proving their hyperbolic nature during the transit in the Hill's sphere for values of μ below a given threshold. In the numerical part, we tested the KS algorithm against a standard Cartesian integration and reported the significant advantages in exploiting the regularization, especially in terms of the Hamiltonian conservation in the extended phase-space; additionally, we produced cartographies using the regularized mFLI indicator to portray the loci of initial conditions exhibiting multiple fast close encounters with P_2 .

CRedit authorship contribution statement

Mattia Rossi: Writing – review & editing, Writing – original draft, Software, Methodology, Investigation, Formal analysis, Data curation.
Massimiliano Guzzo: Writing – review & editing, Writing – original draft, Supervision, Methodology, Investigation, Funding acquisition, Formal analysis, Conceptualization.

Declaration of competing interest

The authors declare that they have no known competing financial interests or personal relationships that could have appeared to influence the work reported in this paper.

Data availability

Physical/orbital data of the planets used for numerical simulations are openly available at nssdc.gsfc.nasa.gov/planetary/factsheet/. The data used to support our findings are included in the paper.

Acknowledgments

The author M.R. acknowledges the project “AIxtreme: Physics-driven AI approaches for predicting extreme weather and space weather events” funded by Compagnia di San Paolo Foundation. The author M.G. acknowledges the project MIUR-PRIN 2020RC5H82 titled “Modern challenges of Celestial Mechanics: from the fundamental theorems to the new models of Planetary Sciences and back”.

Appendix. From the rotating–pulsating to the inertial reference frame

In the ER3BP the primary and the secondary bodies rotate non-uniformly around their common center of mass and have constantly varying relative distance. The rotating–pulsating frame $Oxyz$ then represents the straightforward extension of the synodic frame of the circular case by:

- (i) rotating by $f(t)$, thus with non-constant angular speed \dot{f} ;
- (ii) pulsating in order to rescale lengths by a factor $1/\varrho(f(t))$, where

$$\varrho(f) = \frac{1 - \varepsilon^2}{1 + \varepsilon \cos f} \quad (81)$$

is the primaries' Keplerian ellipse according to units in Section 1.

In this way P_1 and P_2 appear at rest and $\|P_2 - P_1\| = 1$.

The two prescriptions translate mathematically in the application of a rotation matrix $\mathcal{R}(f) \in SO(3)$ and the scaling factor $\varrho(f)$ to a vector $r = (x, y, z) \in \mathbb{R}^3$ in $Oxyz$ to retrieve a vector $R = (X, Y, Z) \in \mathbb{R}^3$ in the inertial frame $OXYZ$:

$$R = \varrho(f)\mathcal{R}(f)r, \quad (82)$$

where

$$\mathcal{R}(f) = \begin{pmatrix} \cos f & -\sin f & 0 \\ \sin f & \cos f & 0 \\ 0 & 0 & 1 \end{pmatrix}. \quad (83)$$

References

- [1] G.D. Birkhoff, The restricted problem of three bodies, *Rend. Circ. Mat. Palermo* (1884-1940) 39 (1) (1915) 265.
- [2] T. Levi-Civita, Sur la régularisation qualitative du problème restreint des trois corps, *Acta Math.* 30 (1906) 305–327.
- [3] P. Kustaanheimo, Spinor regularization of the Kepler motion, *Ann. Univ. Turkuensis A* 73 (1964) 1–7.
- [4] P. Kustaanheimo, E.L. Stiefel, Perturbation theory of Kepler motion based on spinor regularization, *J. Reine Ang. Math.* 218 (1965) 204–219–569.
- [5] E.L. Stiefel, G. Scheifele, *Linear and Regular Celestial Mechanics*. Grundlehren der Mathematischen Wissenschaften, Springer, Berlin, 1971.
- [6] S.J. Aarseth, K. Zare, A regularization of the three-body problem, *CM & DA* 10 (1974) 185–205.
- [7] D.C. Heggie, A global regularization of the gravitational N-body problem, *CM & DA* 10 (1974) 217–241.
- [8] V.A. Shefer, Application of KS-transformation in the problem of investigation of the motion of unusual minor planets and comets, *CM & DA* 49 (1990) 197–207.
- [9] C. Falcolini, Perturbative methods in regularization theory, in: C. Benest (Ed.), *Singularities in Gravitational Systems*, in: *Lecture Notes in Physics*, vol. 590, Springer, Berlin, Heidelberg, 2002.
- [10] S.J. Aarseth, *Gravitational N-Body Simulations, Tools and Algorithms*, Cambridge Univ. Press, New York, 2003.
- [11] J. Waldvogel, Quaternions and the perturbed Kepler problem, *CM & DA* 95 (2006) 201–212.
- [12] K. Langner, S. Breiter, KS variables in rotating reference frame. Application to cometary dynamics, *Astrophys. Space Sci.* 357 (2015) 153.
- [13] S. Breiter, K. Langner, Kustaanheimo-Stiefel transformation with an arbitrary defining vector, *CM & DA* 128 (2017) 323–342.
- [14] V. Szebehely, *Theory of Orbits: The Restricted Problem of Three Bodies*, Elsevier, 2012.
- [15] R.I. Paez, M. Guzzo, Transits close to the Lagrangian solutions L_1 , L_2 in the elliptic restricted three-body problem, *Nonlinearity* 34 (2021) 6417–6449.
- [16] V. Szebehely, G.E.O. Giacaglia, On the elliptic restricted problem of three bodies, *Astron. J.* 69 (1964) 230.
- [17] R. Broucke, Periodic collision orbits in the elliptic restricted three-body problem, *CM & DA* 3 (1971) 461–477.
- [18] C. Pinyol, Ejection-collision orbits with the more massive primary in the planar elliptic restricted three-body problem, *CM & DA* 61 (1995) 315–331.
- [19] J. Waldvogel, Die Verallgemeinerung der Birkhoff-regularisierung für das räumliche Dreikörperproblem (Ph.D. thesis), ETH Zurich, 1966.
- [20] J. Waldvogel, The restricted elliptic three-body problem, in: E. Stiefel, M. Rössler, J. Waldvogel, C.A. Burdet (Eds.), *Methods of Regularization for Computing Orbits in Celestial Mechanics*. NASA Contractor Report NASA CR, Vol. 769, 1967, pp. 88–115.
- [21] R.F. Arenstorf, Regularization theory for the elliptic restricted three body problem, *J. Differential Equations* 6 (3) (1969) 420–451.
- [22] J. Llibre, C. Piñol, On the elliptic restricted three-body problem, *CM & DA* 48 (1990) 319–345.
- [23] F. Cardin, M. Guzzo, Integrability of close encounters in the spatial restricted three-body problem, *Comm. Cont. Math.* 24 (06) (2022) 2150040.
- [24] M. Guzzo, E. Lega, A study of the past dynamics of comet 67P/Churyumov-Gerasimenko with fast Lyapunov indicators, *Astron. Astrophys.* 579 (A79) (2015) 1–7.
- [25] M. Guzzo, E. Lega, Scenarios for the dynamics of comet 67P/Churyumov-Gerasimenko over the past 500 kyr, *Mon. Not. R. Astron. Soc.* 469 (2017) S321–S328.
- [26] J. Henrard, On Poincaré's second species solutions, *CM & DA* 21 (1980) 83–97.
- [27] J. Font, A. Nunes, C. Simó, Consecutive quasi-collisions in the planar circular RTBP, *Nonlinearity* 15 (2002) 115.
- [28] M. Guzzo, E. Lega, On the identification of multiple close-encounters in the planar circular restricted three body problem, *Mon. Not. R. Astron. Soc.* 428 (2013) 2688–2694.
- [29] M. Guardia, V. Kaloshin, J. Zhang, Asymptotic density of collision orbits in the restricted circular planar 3 body problem, *Arch. Ration. Mech. Anal.* 233 (2) (2019) 799–836.
- [30] M. Guzzo, Parametric approximations of fast close encounters of the planar three-body problem as arcs of a focus-focus dynamics, 2023, arXiv preprint arXiv:2311.17108.
- [31] E.J. Öpik, *Interplanetary Close Encounters*, Elsevier, New York, 1976.
- [32] G.B. Valsecchi, Close encounters in öpik theory, in: D. Benest, C. Froeschlé (Eds.), *Singularities in Gravitational Systems*, in: *Lecture Notes in Physics*, Springer, 2002.
- [33] A. Celletti, E. Lega, L. Stefanelli, C. Froeschlé, Some results on the global dynamics of the regularized restricted three-body problem with dissipation, *CM & DA* 109 (2011) 265–284.
- [34] E. Lega, M. Guzzo, C. Froeschlé, Detection of close encounters and resonances in three-body problems through Levi-Civita regularization, *Mon. Not. R. Astron. Soc.* 418 (2011) 107–113.
- [35] M. Guzzo, E. Lega, Theory and applications of fast Lyapunov indicators to model problems of celestial mechanics, *CM & DA* 135 (4) (2023) 37.
- [36] E. Lega, M. Guzzo, Three-dimensional representations of the tube manifolds of the planar restricted three-body problem, *Physica D* 325 (2016) 41–52.
- [37] M. Guzzo, E. Lega, Geometric chaos indicators and computations of the spherical hypertube manifolds of the spatial circular restricted three-body problem, *Physica D* 373 (2018) 38–58.
- [38] M. Rossi, C. Efthymiopoulos, Relegation-free closed-form perturbation theory and the domain of secular motions in the restricted three-body problem, *CM & DA* 135 (4) (2023) 42.
- [39] M. Rossi, C. Efthymiopoulos, Characterization of the stability for trajectories exterior to jupiter in the restricted three-body problem via closed-form perturbation theory, *Proc. Int. Astron. Union* 15 (S364) (2019) 232–238.
- [40] W. Scheibner, Satz aus der störungstheorie. (auszug aus einem schreiben an den herausgeber), *J. Reine Angew. Math.* 1866 (65) (1866) 291–292.
- [41] J. Marsden, A. Weinstein, Reduction of symplectic manifolds with symmetry, *Rep. Math. Phys.* 5 (1) (1974) 121–130.
- [42] K.R. Meyer, *Symmetries and Integrals in Mechanics. Dynamical Systems*, Academic Press, 1973, pp. 259–272.
- [43] P. Saha, Interpreting the Kustaanheimo-Stiefel transform in gravitational dynamics, *Mon. Not. R. Astron. Soc.* 400–1 (2009) 228–231.
- [44] L. Zhao, Kustaanheimo-stiefel regularization and the quadrupolar conjugacy, *Regul. Chaotic Dyn.* 20–1 (2015) 19–36.
- [45] C. Froeschlé, Numerical study of dynamical systems with three degrees of freedom I. Graphical displays of four-dimensional sections, *Astron. Astrophys.* 4 (1970) 115–128.
- [46] H.A. Luther, An explicit sixth-order Runge–Kutta formula, *Math. Comp.* 22 (102) (1968) 434–436.
- [47] M. Guzzo, E. Lega, Evolution of the tangent vectors and localization of the stable and unstable manifolds of hyperbolic orbits by fast Lyapunov indicators, *SIAM J. Appl. Math.* 74 (4) (2014) 1058–1086.